INTERNATIONAL JOURNAL OF CLIMATOLOGY
Int. J. Climatol. (2016)
Published online in Wiley Online Library
(wileyonlinelibrary.com) DOI: 10.1002/joc.4916

RMetS
Royal Meteorological Society

Life cycles of agriculturally relevant ENSO teleconnections in North and South America

Weston Anderson,[a,b]* Richard Seager,[b] Walter Baethgen[c] and Mark Cane[b]

[a] *Department of Earth and Environmental Sciences, Columbia University, New York, NY, USA*
[b] *Lamont-Doherty Earth Observatory, Columbia University, New York, NY, USA*
[c] *Regional and Sectorial Research Program, International Research Institute for Climate and Society, New York, NY, USA*

ABSTRACT: The characteristic evolution of El Niño Southern Oscillation (ENSO) on timescales of months to years means that risks to agriculture have structure between seasons and years. The potential for consecutive ENSO-induced yield anomalies is of particular interest in major food producing areas, where modest changes in yield have significant effects on global markets. In this study, we analyse how multi-year El Niño and La Niña life cycles relate to climate sensitive portions of major crop-growing seasons in North and South America.

We analyse the dynamics underlying these life cycles to illustrate which aspects of the system are most important for agriculture. In North America, the same-season teleconnections affecting soybean and maize have been well studied, but we demonstrate the importance of lagged soil moisture teleconnections for wheat in the southern Great Plains. In South America, peak ENSO sea surface temperature (SST) teleconnections are concurrent with, and therefore critical for, wheat and maize growing seasons while soil moisture memory in Argentina plays an important role during the soybean growing season.

Finally, we show that ENSO teleconnection life cycles are consistent with historical yield anomalies. Both El Niño and La Niña life cycles tend to force consecutive seasons of either above or below expected yields. While the magnitude of the yield anomalies forced by ENSO is often modest, they occur in major crop-producing regions.

KEY WORDS La Niña; maize; wheat; soybean; ENSO; agriculture; America; El Niño Southern Oscillation

Received 26 May 2016; Revised 30 August 2016; Accepted 10 September 2016

1. Introduction

The El Niño Southern Oscillation (ENSO) refers to a coupling between equatorial Pacific Ocean and atmosphere anomalies. Although it is fundamentally a tropical Pacific phenomena, both warm (El Niño) and cold (La Niña) events alter atmospheric circulations – and subsequently temperature and precipitation patterns – well into the midlatitudes (Trenberth *et al.*, 1998; Alexander *et al.*, 2002).

ENSO has proven to be a major driver of global crop yield variability, although its impacts on agriculture in a given year are not uniform (Iizumi *et al.*, 2013). Instead, ENSO tends to create agricultural winners and losers. In an El Niño year, drought is likely in many tropical countries while wetter, milder conditions prevail in the northern hemisphere midlatitudes (Diaz *et al.*, 2001; Mason and Goddard, 2001). Because every ENSO event is slightly different, however, the consistency and timing of these impacts varies between events (Capotondi *et al.*, 2015).

There is the potential to improve regional and global food security through advanced planning by exploiting robust climate teleconnections in major food producing regions of North and South America. While climate is by no means the single determinant of global food security, unexpected declines in the production of staple crops due to poor growing conditions in major producing regions has contributed to food crises in the recent past (FAO, 2009, 2010). Table 1 illustrates that the reported relation between yield anomaly and ENSO phase is generally consistent across studies despite differences in available data and analytical methods. Although most studies have focused on maize in North America and on maize or soybean in South America, ENSO has a significant impact on maize, soybean and wheat yields in both North and South America. Understanding ENSO teleconnections therefore presents the possibility of providing governments, extension officers and farmers with improved information on seasonal timescales (Messina *et al.*, 1999; Podesta *et al.*, 2002; Iizumi *et al.*, 2013). While understanding seasonal climate variability is only the first step towards managing climate-induced risks to food security, it is the foundation upon which effective mitigation practices and policies are built. For a detailed review of how information on climate variability can be used at both the farm and national scale, see Hammer *et al.* (2001) and for a more complete case study of how climate forecasts can improve profit and reduce risks in agriculture, see Hammer *et al.* (1996).

In the past two decades, we have seen tremendous progress towards a robust understanding of ENSO

* Correspondence to: W. Anderson, Lamont-Doherty Earth Observatory, 61 Route 9W, Palisades, New York, NY 10964, USA. E-mail: weston@ldeo.columbia.edu

Table 1. Previous studies of ENSO and crop yield anomalies.

Region	Years	Methods	Crop	Results	Citation
Central-east Argentina (Pergamino and Pilar)	1931–1996	DSSAT (CERES-Maize) crop model	Maize	EN+, LN−	Ferreyra *et al.*, 2001
Central-east Argentina	1900–1999, 1972–1999	Tercile analysis, correlation, PCA	Maize	EN+, LN−	Podestá *et al.*, 1999
			Soybean	LN−	
			Wheat	not significant	
Brazil	1920–1997	Composite analysis	Wheat	EN−, LN+	Cunha *et al.*, 2001
Global (southeast South America)	1984–2004	Composite analysis	Maize	EN+, LN−	Iizumi *et al.*, 2014
			Soybean	EN+, LN−	
			Wheat	EN+/−, LN+	
Global (Mexico, US)	1984–2004	Composite analysis	Maize	EN−, LN−	Iizumi *et al.*, 2014
			Soybean	EN+	
			Wheat	not significant	
North America (US and Mexico)	1960–1989, 1970–1989	EPIC crop model	Maize	EN+/−	Izaurralde *et al.*, 1999[a]
North America (US)			Wheat	EN+/−	
Oaxaca, Mexico	1978–1990	Regression analysis	Maize	EN−, LN+	Dilley, 1997
Mexico	1960–1989	EPIC crop model, composite analysis	Maize	EN+/−, LN+/−	Lopez *et al.*, 2003[a]
United States	–	EPIC crop model	Maize	LN−	Legler and Bryant, 1999[a]
			Soybean	EN−, LN−	
			Wheat	not significant	
United States	1868–1982	Regression analysis	Maize	EN+, LN−	Handler, 1984
United States	1950–1995	Lagged regression analysis and DSSAT (CERES-Maize) crop model	Maize	LN−	Phillips *et al.*, 1999
United States	1909–1994	Quartile composite analysis	Wheat	EN+, LN−	Mauget and Upchurch, 1999
United States	1982–1997	Quartile composite analysis	Maize	EN+, LN−	Wannebo and Rosenzweig, 2003
Canadian Prairie	1960–1997	Regression analysis, PCA of SSTs, composite analysis	Spring wheat	EN+, LN+/−	Hsieh *et al.*, 1999

[a]These studies looked at spatial patterns, not production weighted yield anomalies.

teleconnections, but there are still agriculturally relevant aspects of the system that are poorly understood. For example, the relationship between crop yields and ENSO is often implicitly treated as annually independent. However, the dynamics underpinning ENSO produce a characteristic evolution from one phase to another (Rasmusson and Carpenter, 1982; Okumura and Deser, 2010). This multi-year evolution raises the question of whether ENSO poses risks or benefits to consecutive cropping seasons which, in a global economy, are important for market prices and global food security. As such, this study explores the extent to which El Niño and La Niña demonstrate a robust life cycle of agriculturally relevant teleconnections.

1.1. ENSO life cycle

At the heart of ENSO is the Bjerknes feedback. In the equatorial Pacific, prevailing easterly winds lift the thermocline in the east, bringing cold upwelling water to the surface, and accumulate warm surface water in the west, which leads to a zonal sea surface temperature (SST) gradient. These zonal SST gradients reinforce easterly winds, and carry water vapour into the west Pacific warm pool to fuel deep convection, a process that increases upwelling in the east and completes the positive (Bjerknes) feedback (Bjerknes, 1969). When the easterly trades relax, the positive feedback can run in the opposite direction to create anomalous warming in the east: El Niño conditions. These

Table 2. Flowering dates by continent and season.

	North America		South America	
	First season	Second season	First season	Second season
Wheat	AMJ	JJA	SON	–
Maize	JJA	–	NDJ	JFM
Soybean	JJA	–	JFM	–

El Niño events tend to last 1–2 years and reoccur every 3–7 years. While there is still debate as to whether ENSO is a self contained oscillatory mode or a stable response to stochastic wind forcing, both theories agree that ENSO is strongly modified, and to some extent phase locked, with the seasonal cycle (Thompson and Battisti, 2000; Wang and Picaut, 2004). Both El Niño and La Niña develop in late boreal spring and peak at the end of the calendar year. Rasmusson and Carpenter (1982) were the first to identify a characteristic multi-year life cycle of SST and zonal wind anomalies during El Niño events. Building on their work, subsequent authors have identified similar life cycles for La Niña events, although the spatial structure and seasonal evolution differ somewhat between warm and cold events (Okumura and Deser, 2010). In our analysis of the evolution of ENSO teleconnections, we therefore evaluate life cycles for warm and cold phases of ENSO separately.

1.2. Crop stress-sensitivity

The biological response of plants to abiotic stressors, such as extreme heat and drought, depend on the specifics of the stress, the cultivar and the developmental stage at which the stress is applied. While cereals exhibit some degree of sensitivity to abiotic stress at all stages of growth, the final yield of the crop is most stress-sensitive during the periods around flowering and around grain filling (Barnabás *et al.*, 2008). The time around flowering, which determines the number of grains per planted area, is considered more crucial for cereal crop yields than is grain filling, which determines the weight of the grain. As such, our analysis will focus on the flowering portion of the growing season for each crop. The major flowering seasons for North American crops are the late boreal spring and summer: April, May, June (AMJ) for wheat; June, July, August (JJA) for maize and soybean. Flowering seasons in South America are primarily September, October, November (SON) for wheat, November, December, January (NDJ) for maize and January, February, March (JFM) for soybean. Table 2 lists the major flowering dates by crop and continent.

Our analysis is organized as follows: We present the data in Section 1.3 and discuss the methods used to create the composite ENSO life cycles, which are used to identify both concurrent and lagged teleconnections, in Section 2. In Section 3, we analyse the evolution of relevant teleconnections for each major crop-growing season, and demonstrate that these teleconnections are consistent with observed crop yield anomalies. In Section 5, we summarize our conclusions and discuss their importance.

1.3. Data

We aggregate daily mean atmospheric variables from the NCEP-NCAR Reanalysis I up to monthly quantities for geopotential height, vertical ascent, wind vectors, precipitable water and maximum temperature on a T62 Gaussian grid for the years 1948–2013 (Kalnay *et al.*, 1996). For monthly soil moisture, latent heat and sensible heat, we use the 1.0×1.0 spaced Noah land surface model version 2.0 from the Global Land Data Assimilation System (GLDAS) for the years 1948–2010 (Rodell and Kato Beaudoing, 2015). Due to the truncated availability of the GLDAS data, the 2010 composite had to be removed from the La Niña ensemble in the soil moisture analyses. We use 1.0×1.0 monthly precipitation data from the Global Precipitation Climatology Centre (GPCC) and monthly SST anomaly data from the 2.0×2.0 Extended Reconstructed Sea Surface Temperature version 3b (ERSSTv3b), both for 1948–2013 (Smith *et al.*, 2008; Schneider *et al.*, 2011). El Niño and La Niña events were selected using the Oceanic Niño index, which is a 3-month running mean of SST anomalies in the Niño 3.4 region (http://www.cpc.ncep.noaa.gov/products/analysis_monitoring/ensostuff/ensoyears_ERSSTv3b.shtml). Crop statistics for the United States for 1949–2013 were downloaded from the US Department of Agriculture, National Agricultural Statistics Service (http://quickstats.nass.usda.gov/, accessed 6 August 2015). For Argentina, crop statistics were available for 1969–2010 from the Integrated Agricultural Information System (http://www.siia.gov.ar/). Crop production data in Brazil were available from 1976–2014, and were downloaded from the Brazilian Companhia Nacional de Abastecimento (http://www.conab.gov.br/index.php). Wheat yield data for Canada from 1950 to 2012 was downloaded from the CANSIM database, provided by Statistics Canada (http://www5.statcan.gc.ca/cansim). Maize production data from 1950 to 2008 in Mexico was downloaded from the INEGI Information Databank (http://www3.inegi.org.mx/sistemas/biinegi/). For spatial information on cropland extent in North and South America, a combination of three data sets was used: The Global Agro-Ecological Zones model, the Monthly Irrigated and Rainfed Crop Area data set and the Spatial Production and Allocation Model (Fischer *et al.*, 2008; Portmann *et al.*, 2010; You *et al.*, 2014). Any cell containing above 0.5% cropland in any of the three data sets is indicated as 'major cropped area', whereas all other cells containing cropped area fall under 'minor cropped area'. This combined data set was created as a conservative solution to the significant discrepancies in cropland extent and cropping intensity between data sets (Fritz *et al.*, 2011; Anderson *et al.*, 2015).

2. Methods

2.1. ENSO ensemble composite construction

An ensemble of El Niño and La Niña composites was constructed from years in which the mean boreal wintertime (October, November, December) SST anomaly amplitude

in the Niño 3.4 region exceeded 1 of 2 standard deviation. This threshold corresponds to an absolute departure in SSTs of just under 0.5 C. Following the identification of the events, the calendar years corresponding to the event, prior to the event and following the event were used to construct a complete 'life cycle' composite. The calendar years for the composites will hereafter be referred to as EN −1, EN 0 and EN +1 for the El Niño composite, and as LN −1, LN 0 and LN +1 for the La Niña composite. Years were not allowed to be double counted as an 'event year' (EN 0 or LN 0) in one composite and a previous- or post-event year in another composite of the same ensemble. This would happen, for example, when multiple years in a row meet the selection criteria. In these cases, the composite centred on the first year to meet the selection criteria is used in the ensemble and the composites for the following years are excluded. Figure 1 illustrates the individual composites (shown in grey), as well as the ensemble mean (shown as the thick coloured line).

2.2. Same-season teleconnections

For the southern hemisphere crops that flower during the boreal winter, the climate sensitive portion of the growing season occurs at the same time as peak ENSO SST anomalies. In these cases, ENSO-induced precipitation and maximum temperature anomalies are identified using the previously defined composite years. The mean composite is plotted for areas in which at least 2 out of 3 of the composite members have the same sign as the composite mean. This limits the focus of the analysis to relatively robust teleconnections. Geopotential height, circulation and ascent anomalies are then composited as a means for identifying the dynamics that give rise to each teleconnection. In these dynamical analyses, however, all areas are shaded so as to provide a coherent representation of the atmospheric teleconnections.

2.3. Lagged teleconnections

ENSO teleconnections in boreal spring, during which time SST anomalies are often near neutral, are generally weaker than those in winter and are therefore not likely to play a dominant role in determining growing season temperature and precipitation for spring flowering crops. However, teleconnections during peak ENSO intensity may persist via soil moisture memory and appreciably influence growing season anomalies in the boreal spring. That soil moisture anomalies persist for weeks to months has been documented in models by Delworth and Manabe (1993) and subsequently confirmed in observations by Vinnikov *et al.* (1996). Both studies model soil moisture as a first order Markov process with an exponential autocorrelation function:

$$r(t) = e^{-\frac{t}{T}} \tag{1}$$

where $r(t)$ is the autocorrelation at lag t, and T is the e-folding time for the damping of soil moisture anomalies in the absence of forcing, also referred to as the temporal scale of the autocorrelation. Vinnikov *et al.* (1996) show that T may be reasonably approximated as:

$$T = \frac{1}{\ln\left[\frac{r(1)}{r(2)}\right]} \tag{2}$$

where $r(1)$ is the autocorrelation at a lag of 1 month and $r(2)$ is the autocorrelation at a lag of 2 months. Modelling soil moisture memory as a Markov process assumes that the season in which the anomalies occur is irrelevant. In our analysis, we calculate the characteristic temporal scale of autocorrelation for soil moisture depths 0–10, 10–40 and 40–100 cm to confirm that the soil moisture data demonstrate persistence lasting up to a season. The ability of soil moisture to perpetuate anomalies, therefore, is a necessary but not sufficient condition for boreal wintertime ENSO teleconnections to impact springtime soil moisture. For this to happen, a region must have persistence of soil moisture anomalies from boreal winter to the spring seasons, and ENSO must have a significant wintertime teleconnections to the region.

To estimate the potential impact of previous boreal winter precipitation on subsequent spring soil moisture, we use a partial correlation analysis. The partial correlation between spring soil moisture and previous winter precipitation with the influence of spring precipitation removed ($\rho_{SM_{sp}P_w \bullet P_{sp}}$), for instance, would be calculated as:

$$\rho_{SM_{sp}P_w \bullet P_{sp}} = \frac{\rho_{SM_{sp}P_w} - \rho_{P_wP_{sp}} \times \rho_{P_{sp}SM_{sp}}}{\sqrt{1 - \rho^2_{P_wP_{sp}} \times \rho^2_{P_{sp}SM_{sp}}}} \tag{3}$$

Where $\rho_{SM_{sp}P_w}$ is the correlation between boreal spring soil moisture and winter precipitation, $\rho_{P_wP_{sp}}$ is the correlation between boreal spring and winter precipitation and $\rho_{P_{sp}SM_{sp}}$ is the correlation between spring precipitation and soil moisture. Statistical significance ($p < 0.1$) is assessed accounting for the number of variables on which the correlation is conditioned. From this analysis, we infer the degree to which, in a typical year, boreal winter precipitation anomalies persist through to spring soil moisture. To analyse whether these relationships are relevant in ENSO years, we first translate precipitation anomalies into volumetric estimates of spring soil moisture anomalies. We use a point-wise multiple linear regression model in which boreal spring soil moisture anomalies are regressed against antecedent winter and concurrent spring precipitation anomalies:

$$SM_{sp} = \beta_0 + \beta_1 \times P_w + \beta_2 \times P_{sp} + \varepsilon \tag{4}$$

where SM_{sp} is the current boreal spring soil moisture anomaly, P_w is the previous winter precipitation anomaly, and P_{sp} is the current spring precipitation anomaly. The βs for each parameter indicate the relative strength of each term. Finally, we composite the volumetric estimates of spring soil moisture originating from the previous winter months' precipitation anomalies as was done for the

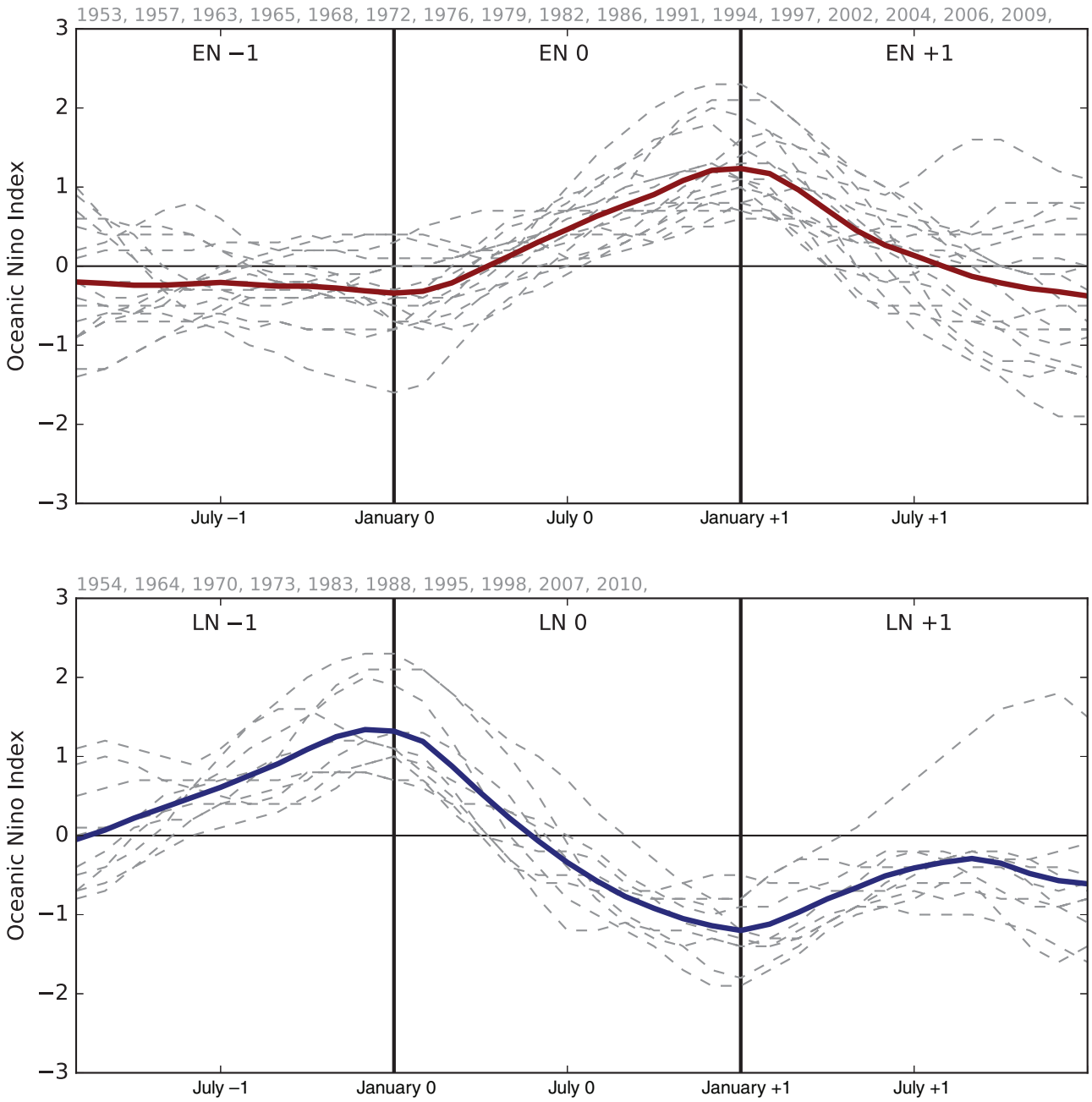

Figure 1. Three year El Niño and La Niña composites of the Oceanic Niño Index, which is calculated as the 3-month running mean of sea surface temperatures in the Niño 3.4 region. Ensemble mean shown in bold. Ensemble event years (EN 0 or LN 0) in grey above each panel.

same-season teleconnections. By performing these three analyses rather than directly compositing spring soil moisture, we are able to separate the relative impact of previous boreal winter precipitation anomalies on spring soil moisture and confirm that observed soil moisture anomalies occur in areas with sufficient soil moisture memory, as opposed to being identified via spurious correlations between precipitation and soil moisture.

2.4. Crop yield anomaly analysis

We use historical yield anomalies to demonstrate that observed ENSO-yield relations are consistent with our derived teleconnections from the previous sections. These relations are analysed in greater detail in previous studies as referenced in Table 1. In this analysis, we consider only states/provinces with an appreciable fraction of national production (>2% of production in 2010). The results are relatively insensitive to the specific threshold chosen to define major producing states. We first correlate SST anomalies with crop yield anomalies to illustrate that the sign of the correlation is consistent with the expected biophysical responses to temperature and precipitation stresses. Yield anomalies were calculated as follows. First expected yields were calculated as the piece-wise linear trends in yield of major crop-producing states/provinces. The trends represent non-climate factors, such as technological advances, which contribute to increases in yield. Deviations from these trends are used to calculate the

anomaly as a percent of expected yield, which is correlated with the Niño 3.4 index. The significance ($p < 0.1$) of the correlations is evaluated following the methods of Ebisuzaki (1997) to account for serial correlation in the data. The final correlation coefficients in all countries are relatively insensitive to the choice of using a piece-wise linear trend (having a breakpoint at 1980) or a linear trend without breakpoints. We then aggregate these state-wise yield anomalies into distributions during each phase of the ENSO life cycle and use a one-tailed Wilcoxon test to identify distributions that are different ($p < 0.1$) from a distribution around zero (Wilks, 2011). The choice of the nonparametric Wilcoxon test, as opposed to the normality assumed in a two-tailed *t*-test, makes little difference in the results.

3. Results

3.1. Same-season teleconnections

3.1.1. South America teleconnections

SST anomalies during the major flowering seasons for wheat (SON), maize (NDJ) and soybean (JFM) evolve slowly, but precipitation anomalies change sign from one season to the next. In the following sections, we will analyse the complete 3-year life cycle of ENSO teleconnections for SON, followed by a discussion of why the atmospheric teleconnections evolve rapidly from SON to JFM, despite SST anomalies remaining fairly constant.

3.1.1.1. Wheat flowering season (SON) teleconnections: Precipitation teleconnections are most robust for the SON season (see Figure 2 for El Niño and Figure 3 for La Niña), when ENSO SST anomalies are at their maximum (see Figure 1). Peak ENSO SST anomalies are associated with a Rossby wave train originating in the tropics and radiating out to the southern tip of South America, often referred to as the Pacific South America mode, which sets up a circulation centred over southeast South America (Mo and Paegle, 2001). Precipitation anomalies associated with this circulation are driven by anomalous vertical motion related to the balance between vortex stretching/compression and advection of planetary vorticity. Areas with poleward flow are associated with vortex stretching and ascent, while areas with equatorward flow are associated with vortex compression and descent. Noting the westward tilt with height of the wave trains, Figures 2 and 3 indicate that areas of wetting (drying) are associated with anomalous poleward (equatorward) lower-level flow. The upper-level anticyclone centred over southeast South America during El Niño therefore results in lower-level poleward flow and wetting over major agricultural areas. This pattern reverses itself during La Niña. These results are consistent with previous analyses of precipitation teleconnections over southeast South America during ENSO events (Grimm *et al.*, 2000; Cazes-Boezio *et al.*, 2003).

3.1.1.2. Maize and soybean flowering season (NDJ and JFM) teleconnections: Owing to the lack of teleconnections during EN −1 (see Figure 2) and the similarity of teleconnections between LN 0 and LN +1 (see Figure 3), we will discuss the evolution of the circulation from SON to JFM for EN 0 and LN 0 only. This seasonal progression is examined because, while the SST forcing remains of the same sign, the upper-level circulation responsible for precipitation teleconnections over southeast South America is established, persists, and dissipates between September and March.

From SON to NDJ, the atmospheric circulation remains much the same for both EN 0 and LN 0 (see Figures 4 and 5), but during JFM of EN 0 (LN 0), the upper-level anticyclone (cyclone) has largely dissipated (Figures 4 and 5). However, the northwesterly anomalies in El Niño years over southeast South America remain, as do the wet anomalies, although they are weaker and limited in extent. In La Niña years, on the other hand, the flow becomes primarily poleward, which leads to anomalous ascent and positive precipitation anomalies in southwest Brazil (Figure 5).

Cunha *et al.* (2001) attribute negative wheat yields in El Niño years to an excess of rainfall, reduced sunshine, and an over-abundance of soil moisture – conditions favourable to the development of disease in wheat crops – while Podestá *et al.* (1999) demonstrate that 3 months later those same wet conditions are beneficial for maize, which requires considerable precipitation and soil moisture during flowering. We therefore expect that South American wheat yields will decrease in response to excess precipitation, while maize and soybean yields will increase in response to excess precipitation.

3.1.2. North America teleconnections

The major flowering season for winter wheat in North America is April, May and June (AMJ). The AMJ season coincides with boreal spring and thus the development or decay of ENSO events. Teleconnections at this time are likely to be weaker than the boreal winter teleconnections observed in the Southern Hemisphere. SST anomalies during June, July, August (JJA) – the critical season for maize and soybean – are also typically weak, providing only modest forcing for summertime teleconnections. Boreal summer basic state flow is also less conducive to strong tropical–extratropical teleconnections (Kumar and Hoerling, 1998). Nevertheless, past studies indicate that JJA teleconnections are important for crop yields (see Table 1).

The magnitude and extent of the AMJ teleconnections are limited (not shown). Precipitation teleconnections are also limited during JJA in the midwest, but patterns of lower maximum temperatures in the summer of a developing El Niño event [EN 0 (not shown), LN −1 in Figure 6] and elevated maximum temperatures in the summer of a developing La Niña event (LN 0; Figure 6) are clear. The regions of elevated maximum temperature anomalies are associated with anticyclonic lower-level flow (Figure 6).

Based on these teleconnections, we expect that La Niñas will depress maize and soybean yields. Although the teleconnections are modest, the relation between maximum temperature and yield is strongly nonlinear (Schlenker and

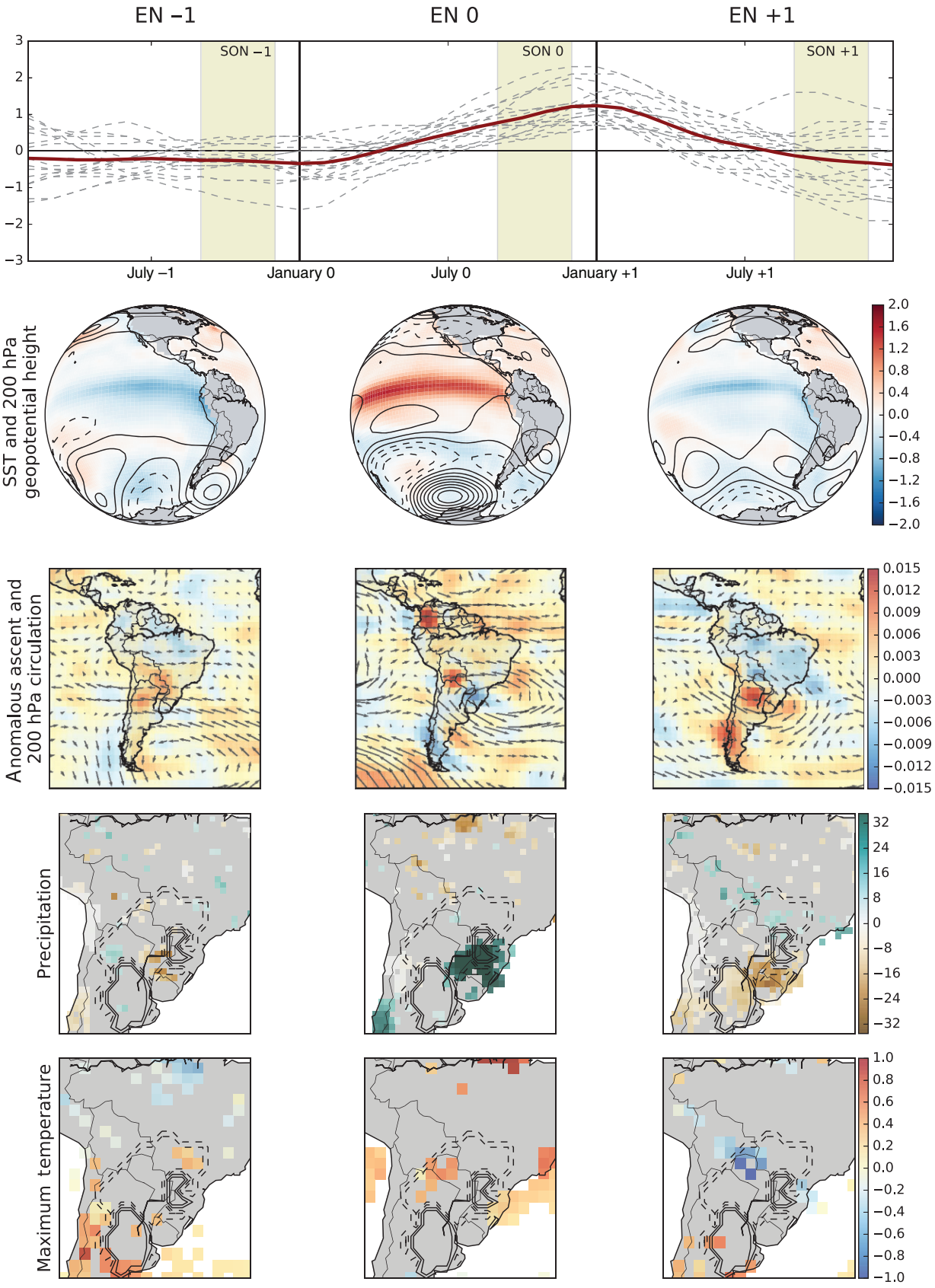

Figure 2. El Niño composite (top row; units C), shading indicates SON growing season. Sea surface temperature anomalies with contours of 200 hPa geopotential height anomalies (second row, contours every 10 hPa), 700 hPa anomalous ascent in pascals per second and 200 hPa circulation anomalies (third row), and seasonal precipitation anomalies in mm month^{-1} (fourth row) and average maximum temperature anomalies in C (fifth row) with contours indicating major (solid) and minor (dashed) wheat growing areas. Each variable is depicted for SON −1 (left column), SON 0 (centre column) and SON +1 (right column).

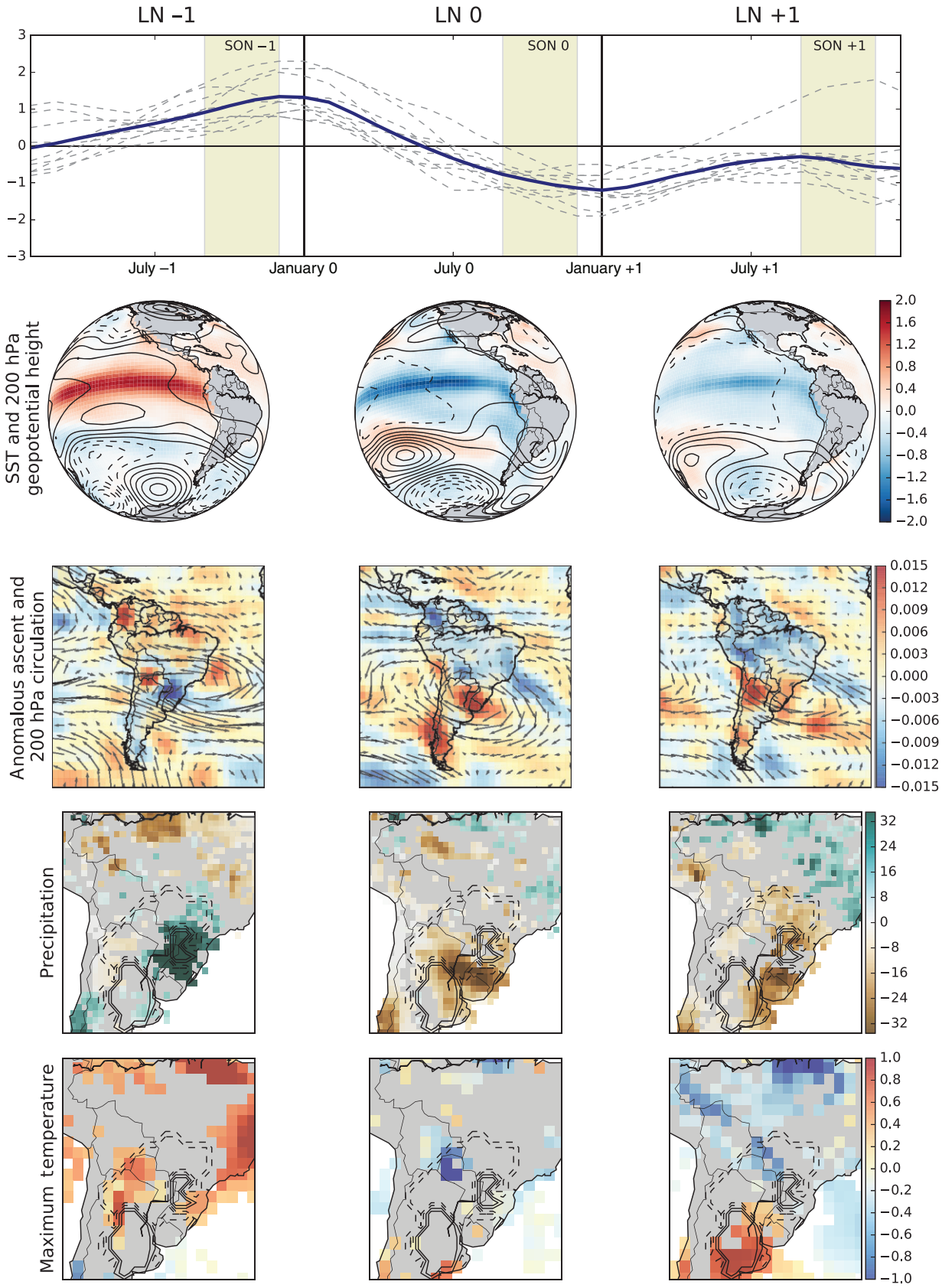

Figure 3. La Niña composite (top row; units C), shading indicates SON growing season. Sea surface temperature anomalies with contours of 200 hPa geopotential height anomalies (second row, contours every 10 hPa), 700 hPa anomalous ascent in pascals per second and 200 hPa circulation anomalies (third row), and seasonal precipitation anomalies in mm month^{-1} (fourth row) and average maximum temperature anomalies in C (fifth row) with contours indicating major (solid) and minor (dashed) wheat growing areas. Each variable is depicted for SON −1 (left column), SON 0 (centre column) and SON +1 (right column).

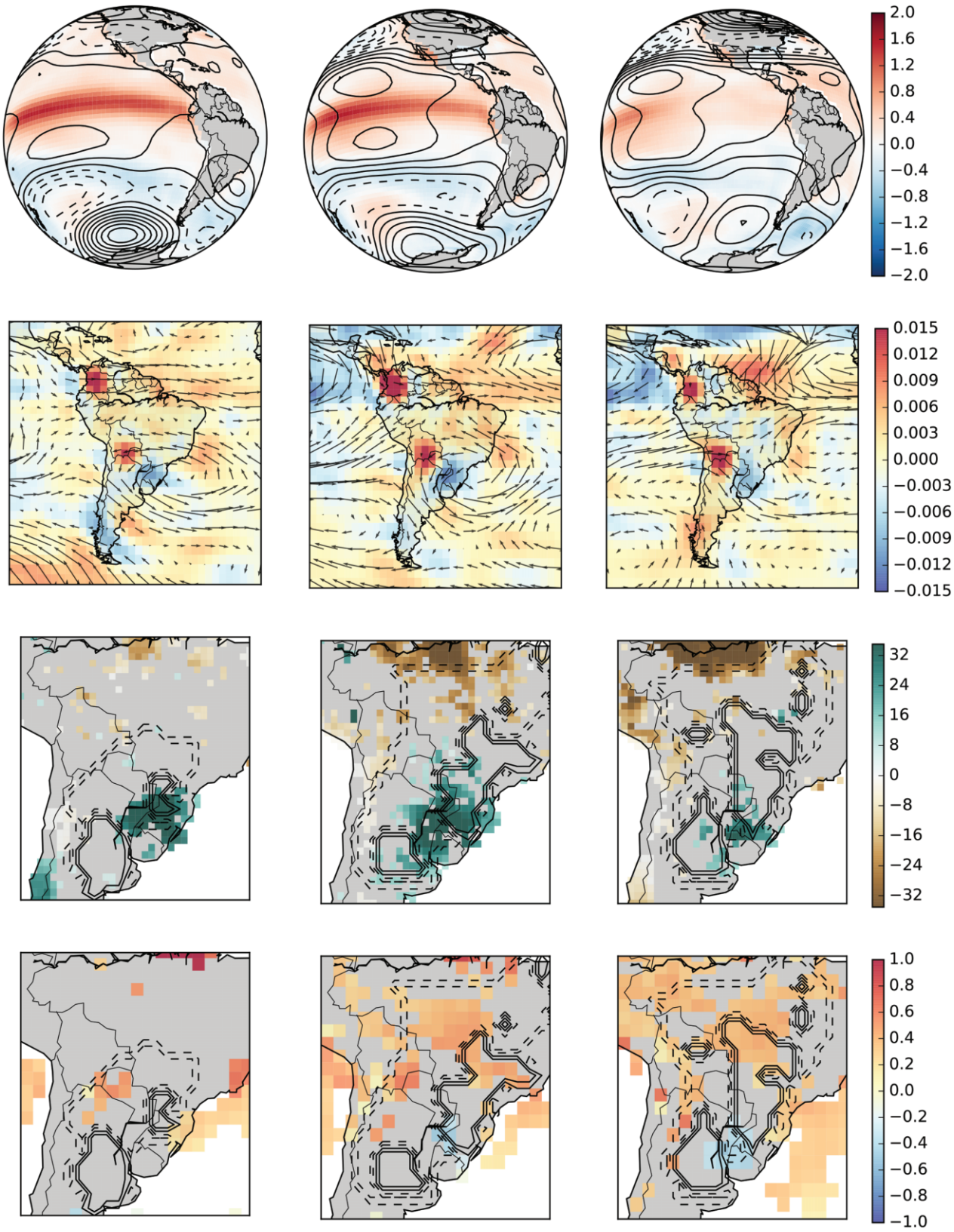

Figure 4. Evolution of peak El Niño teleconnections over the wheat (SON), maize (NDJ) and soybean (JFM) growing seasons. Sea surface temperature anomalies with contours of 200 hPa geopotential height anomalies (first row, contours every 10 hPa), 700 hPa anomalous ascent in pascals per second and 200 hPa circulation anomalies (second row), and seasonal precipitation anomalies in mm month^{-1} (third row) and average maximum temperature anomalies in C (fourth row) with contours indicating major (solid) and minor (dashed) growing area of the dominant crop in each season.

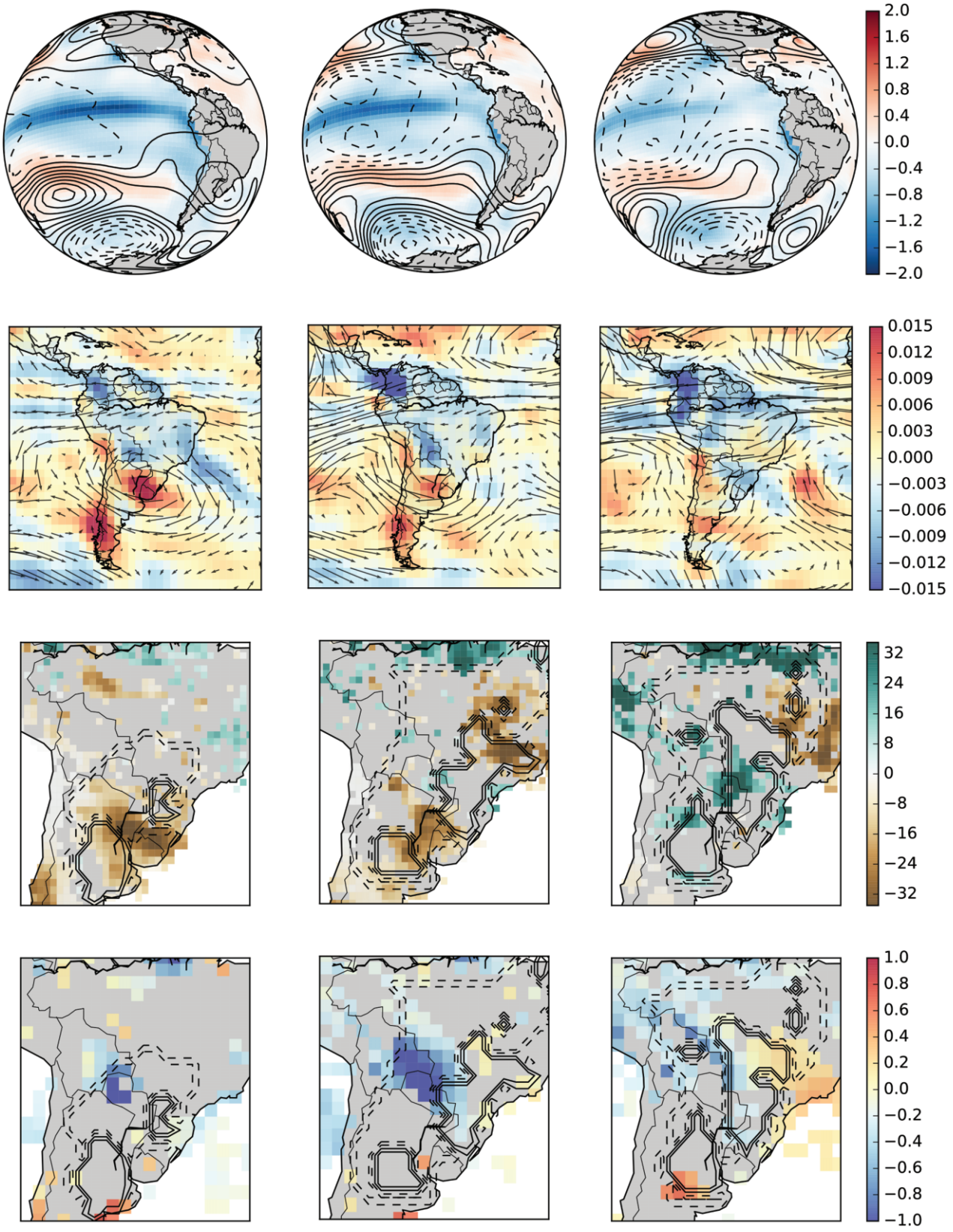

Figure 5. Evolution of peak La Niña teleconnections over the wheat (SON), maize (NDJ) and soybean (JFM) growing seasons. Sea surface temperature anomalies with contours of 200 hPa geopotential height anomalies (first row, contours every 10 hPa), 700 hPa anomalous ascent in pascals per second and 200 hPa circulation anomalies (second row), and seasonal precipitation anomalies in mm month^{-1} (third row) and average maximum temperature anomalies in C (fourth row) with contours indicating major (solid) and minor (dashed) growing area of the dominant crop in each season.

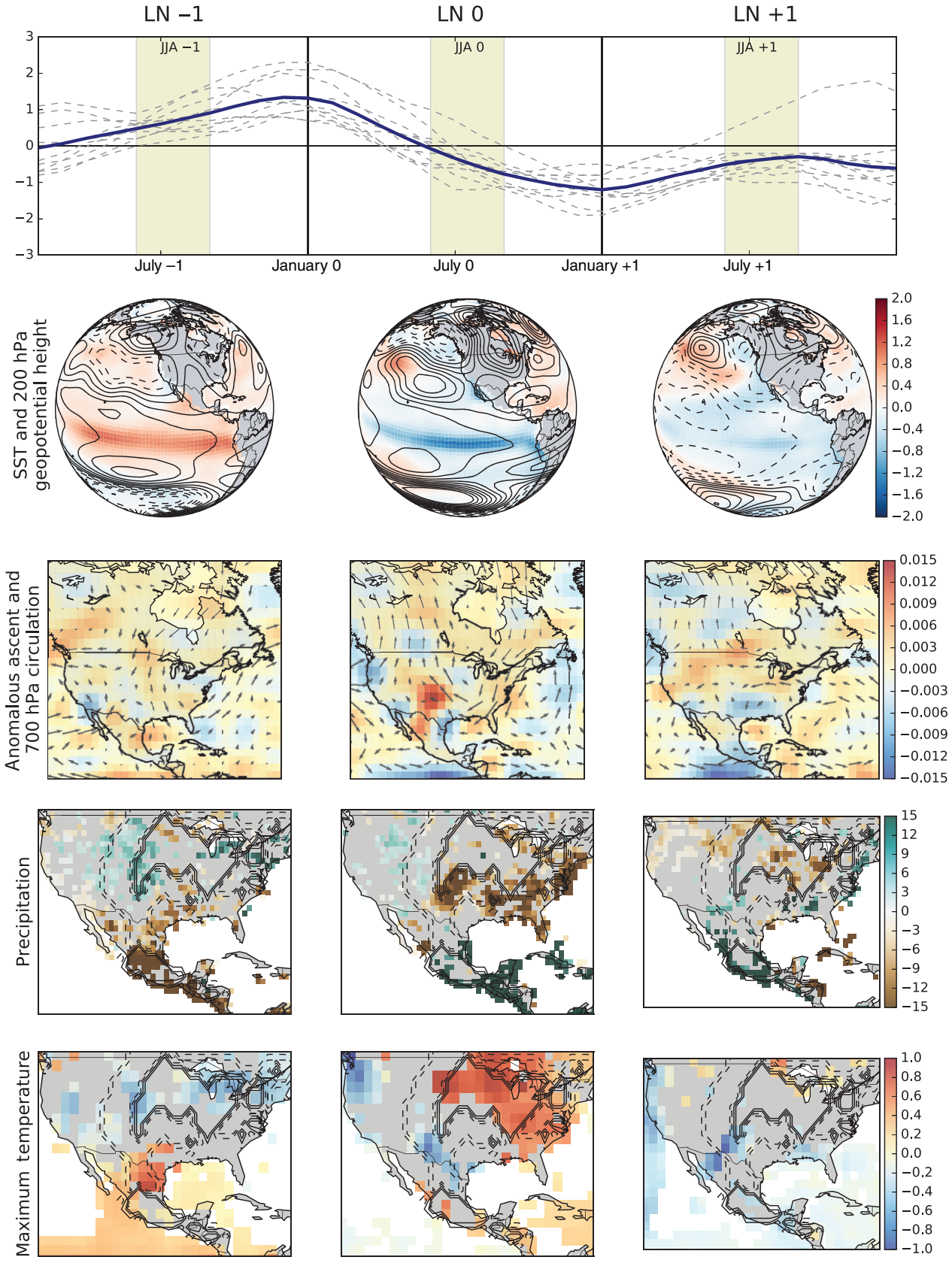

Figure 6. La Niña composite (top row; units C), shading indicates JJA growing season. Sea surface temperature anomalies in C with contours of 200 hPa geopotential height anomalies (second row; contours every 5 hPa), 700 hPa anomalous ascent in pascals per second and circulation anomalies (third row), seasonal precipitation anomalies in mm month^{-1} (fourth row), and average maximum temperature anomalies in C (fifth row) with contours indicating major (solid) and minor (dashed) wheat growing areas. Each variable is depicted for JJA −1 (left column), JJA 0 (centre column) and JJA +1 (right column).

Roberts, 2006, 2009; Lobell *et al.*, 2013, 2014) and as Phillips *et al.* (1999) note, La Niñas tend to bring both moisture stress and elevated temperatures.

3.2. Lagged teleconnections

3.2.1. North America teleconnections

To evaluate whether lagged teleconnections exist, we first calculate soil moisture memory to assess whether a physical pathway for sustaining anomalies exists. We next conduct a partial correlation analysis to analyse the season-specific relations, and finally estimate the magnitude of each lagged teleconnection using a multiple linear regression analysis. As described in the Methods section, we calculated the potential soil moisture memory as the e-folding time for the damping of soil moisture anomalies in the absence of external forcing (see Figure 7, right column). Areas with appreciable soil moisture memory, ranging from 3 months up to 6+ months, coincide remarkably well with major wheat producing regions. These results agree with those of Schubert *et al.* (2004), who demonstrate the relevance of soil moisture for perpetuating long-term droughts in the Great Plains.

Considering that soil moisture memory does not exceed 4 months in the 10–40 cm layer over most of the US, we will consider only the season immediately preceding each flowering season. For wheat, we analyse the influence of boreal mid-winter (DJFM) precipitation anomalies on spring (AMJ) soil moisture, whereas for soybean and maize, we analyse the influence of early spring (FMAM) precipitation anomalies on summer (JJA) soil moisture.

The partial correlation analysis demonstrates that boreal winter precipitation anomalies are significantly ($p < 0.1$) correlated with spring soil moisture anomalies in the Southwest and also the southern Great Plains, an important wheat production area (see Figure 7). While the DJFM correlation holds throughout the soil column, the relative importance of winter to spring precipitation for spring soil moisture increases with depth. Early spring (FMAM) precipitation anomalies are also significantly correlated with summertime (JJA) soil moisture anomalies in regions of major maize and soybean production, although due to weak ENSO teleconnections in the early boreal spring the ENSO influence on summer soil moisture will be weak (not shown).

Soil moisture memory is therefore unimportant for the boreal summer-season crops, but acts to translate ENSO-induced winter precipitation anomalies into spring growing season soil moisture anomalies (see Figures 8 and 9). Potential evapotranspiration is also lower in the spring than in the summer such that soil moisture can more adequately satisfy the water demands of wheat. As in South America, the boreal winter precipitation anomalies co-occur with maximum SST anomalies and are related to a Rossby wave train originating in the tropics and propagating into the midlatitudes. Peak El Niños (third column of Figure 8) are associated with positive precipitation anomalies in the Southwest and southern Great Plains that cause positive soil moisture anomalies to persist into the following growing season. In contrast, during peak La Niña (third column of Figure 9) negative precipitation anomalies persist from boreal winter to spring, consistently decreasing soil moisture and increasing maximum temperatures. We therefore expect that the southern Great Plains states will demonstrate a positive correlation between SST and wheat yields based on these lagged teleconnections.

3.2.2. South America teleconnections

Owing to the strength of same-season teleconnections during the critical flowering season for wheat and maize in South America (SON and NDJ), lagged teleconnections become important only in the soybean flowering season (JFM). The soil moisture memory in South America was assessed in the same manner as that of North America. The e-folding times for soil moisture in northern Argentina, Paraguay and southern Bolivia were around 3 months in the 10–40 cm layer and about 4 months in the 40–100 cm layer, which implies sufficient memory for teleconnections to persist from early boreal winter (SOND) through to JFM (see Figure 10). The partial correlation analysis confirms that although the correlation with concurrent precipitation is greatest at depth in the soil column (Figure 10, left column), there exists a non-trivial partial correlation between JFM soil moisture and previous season precipitation in the same crop-growing regions that demonstrated soil moisture memory.

Figures 11 and 12 illustrate the impact that previous season precipitation has on JFM soil moisture during composite ENSO life cycles. The precipitation forcing remains consistent from SOND into JFM during both the development of El Niño and peak El Niño (see Figure 4). Precipitation anomalies from the previous season (SOND) therefore act to reinforce those of the current season (JFM) during the onset and peak of El Niño, resulting in significant soil moisture anomalies even when the JFM precipitation anomaly is weak.

Precipitation forcing disappears or weakly reverses sign in southeast South America during peak to decaying La Niñas (see Figure 5) and in the year following major La Niñas (not shown). The widespread negative precipitation anomalies in Argentina and Uruguay during SOND (Figure 12, LN +1) disappears following the dissipation of the cyclonic circulation in JFM (see Figure 5 and previous section discussion). However, the dry soil moisture anomalies persist through to total JFM soil moisture anomalies (Figure 12, LN 0 and LN +1). Soil moisture memory may therefore be important for major soybean producing areas in Argentina, leading to positive correlations with SST.

3.2.3. Life cycles of teleconnections

Life cycles of El Niño and La Niña differ in that over the course of a 3-year life cycle of La Niña, there are strong teleconnections in each of the 3 years, while over the equivalent 3-year life cycle of an El Niño, there tends to be only 1 or 2 years with appreciable teleconnections. This discrepancy arises because the strength of ENSO

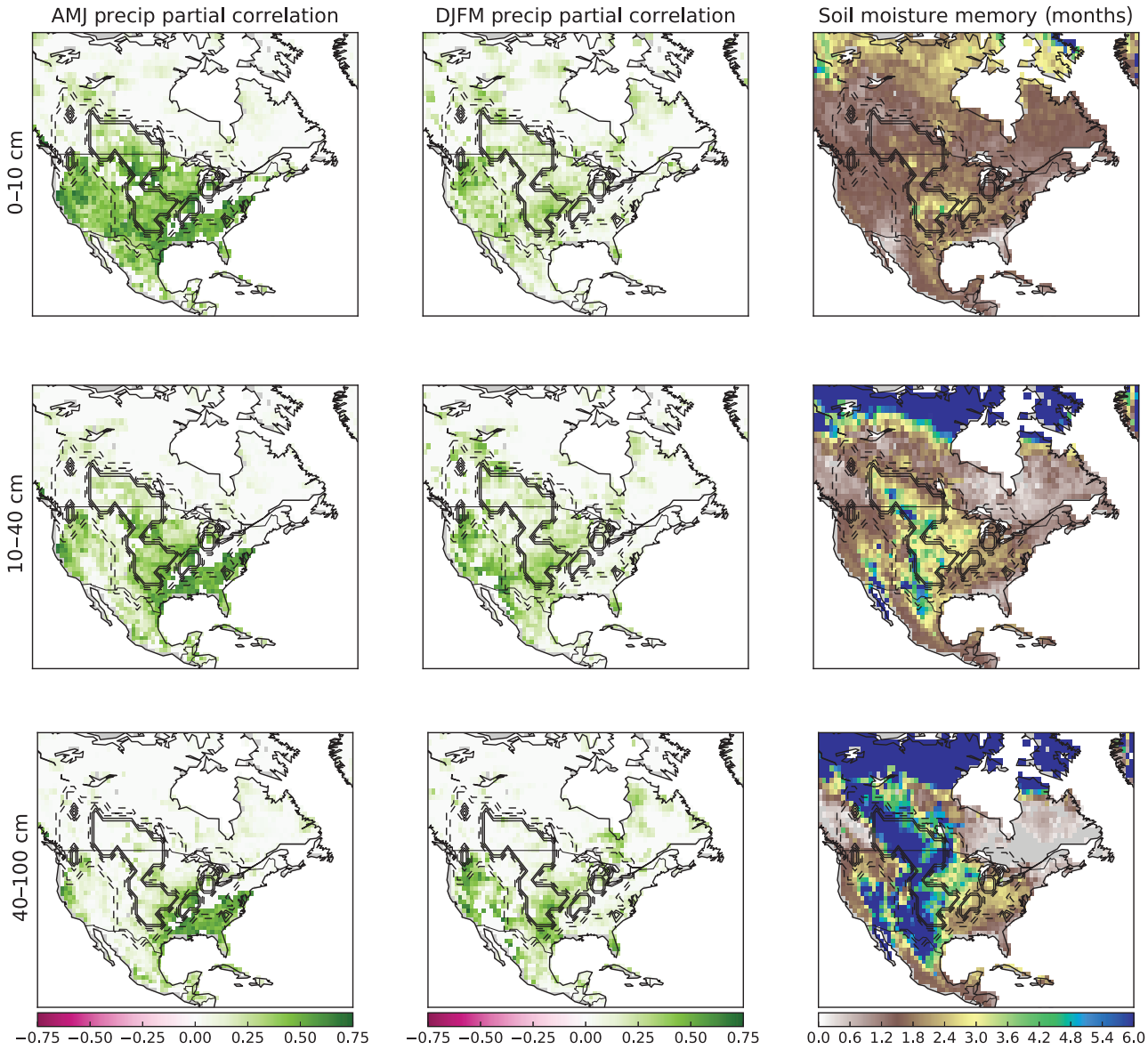

Figure 7. Statistically significant ($p < 0.1$) point-wise partial correlation between AMJ soil moisture and AMJ precipitation (left column) and DJFM precipitation (centre column). The e-folding time in months for soil moisture anomalies in the absence of forcing (right column). Rows indicate soil moisture layer depths of 0–10 cm (top row), 10–40 cm (centre row) and 40–100 cm (bottom row). Contours indicate wheat producing areas.

teleconnections are dependent upon, among other things, the magnitude of concurrent SST anomalies (Kumar and Hoerling, 1998). And while all La Niñas form following El Niños, only about half of all El Niños develop into La Niñas.

The development and decay of an El Niño event lasts nearly 2 years such that two major cropping seasons experience anomalies attributable to El Niño. Teleconnections occurring in EN 0 and EN +1 years tend to have opposite signs to one another. Provided that La Niñas develop following El Niños and persist for 2 years thereafter, there tend to be appreciable teleconnections for three major cropping seasons during a La Niña life cycle. And because cold SST anomalies favour dry conditions in major cropping areas of both North and South America, the La Niña life cycle forces two dry seasons and only one wet season. The southern Great Plains of North America experience wet anomalies during the boreal winter of an El Niño, but experience dry anomalies during the preceding and following winters (see Figure 9). In South America, wet anomalies during the peak of El Niño preceding La Niña are followed by 2 years of negative SSTs and dry anomalies (see Figure 3).

3.3. Teleconnections and yield anomalies

Following from the previous analyses, as well as a much greater body of literature detailing crops' physiological response to precipitation and temperature anomalies during the growing season, we can infer the sign of yield anomalies attributable to El Niño and La Niña. While most crops respond intuitively to moisture and heat, it is worth noting that drying implies opposite wheat yield variability

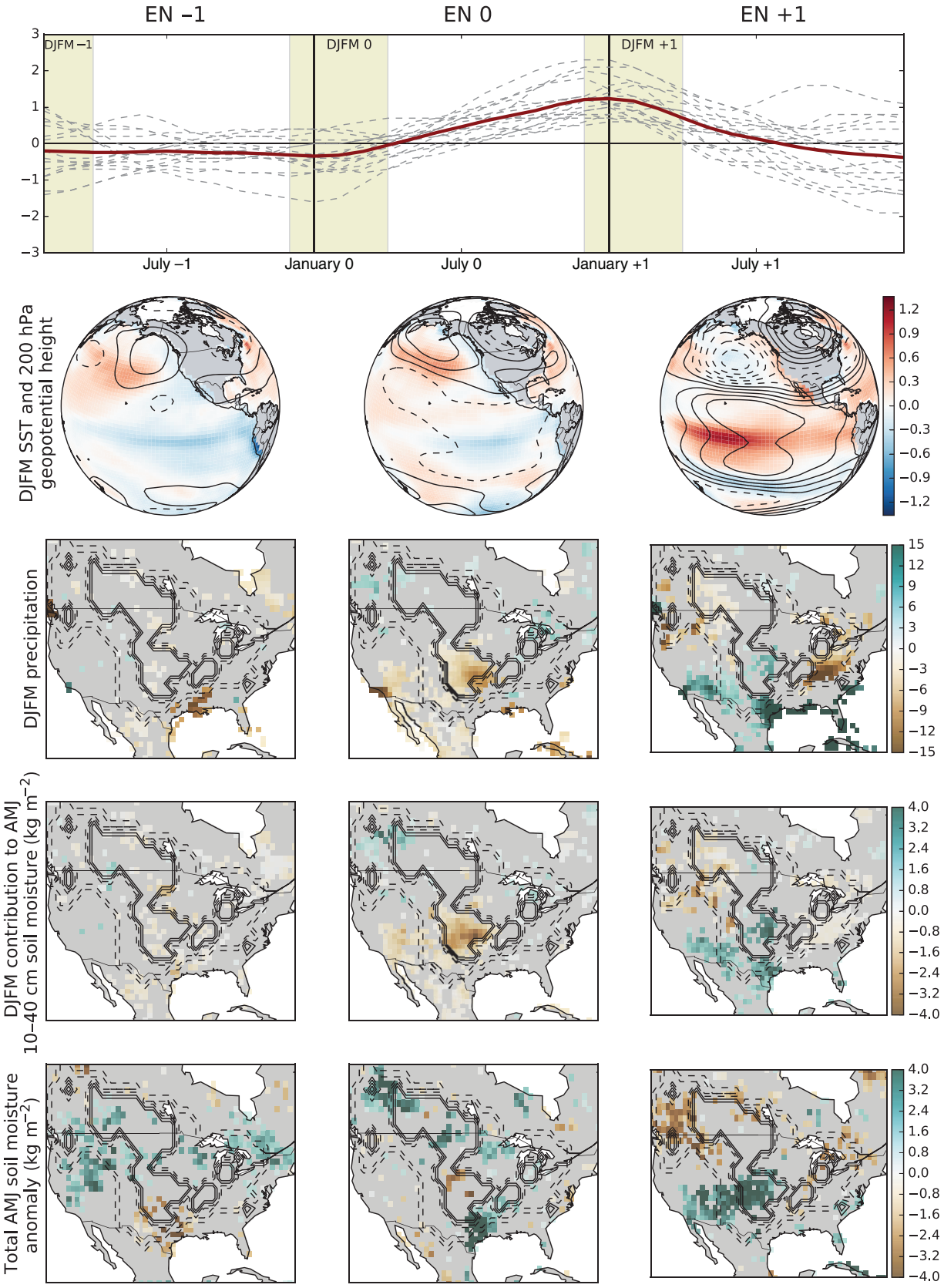

Figure 8. El Niño composite (top row), shading indicates DJFM. Sea surface temperature anomalies with contours of 200 hPa geopotential height (second row), boreal winter precipitation anomalies (third row; units of mm month^{-1}), and boreal winter precipitation contribution to springtime soil moisture (fourth row; units of kg m^{-2}) with contours indicating major (solid) and minor (dashed) wheat growing areas. Each variable is depicted for DJFM −1 (left column), DJFM 0 (centre column) and DJFM +1 (right column).

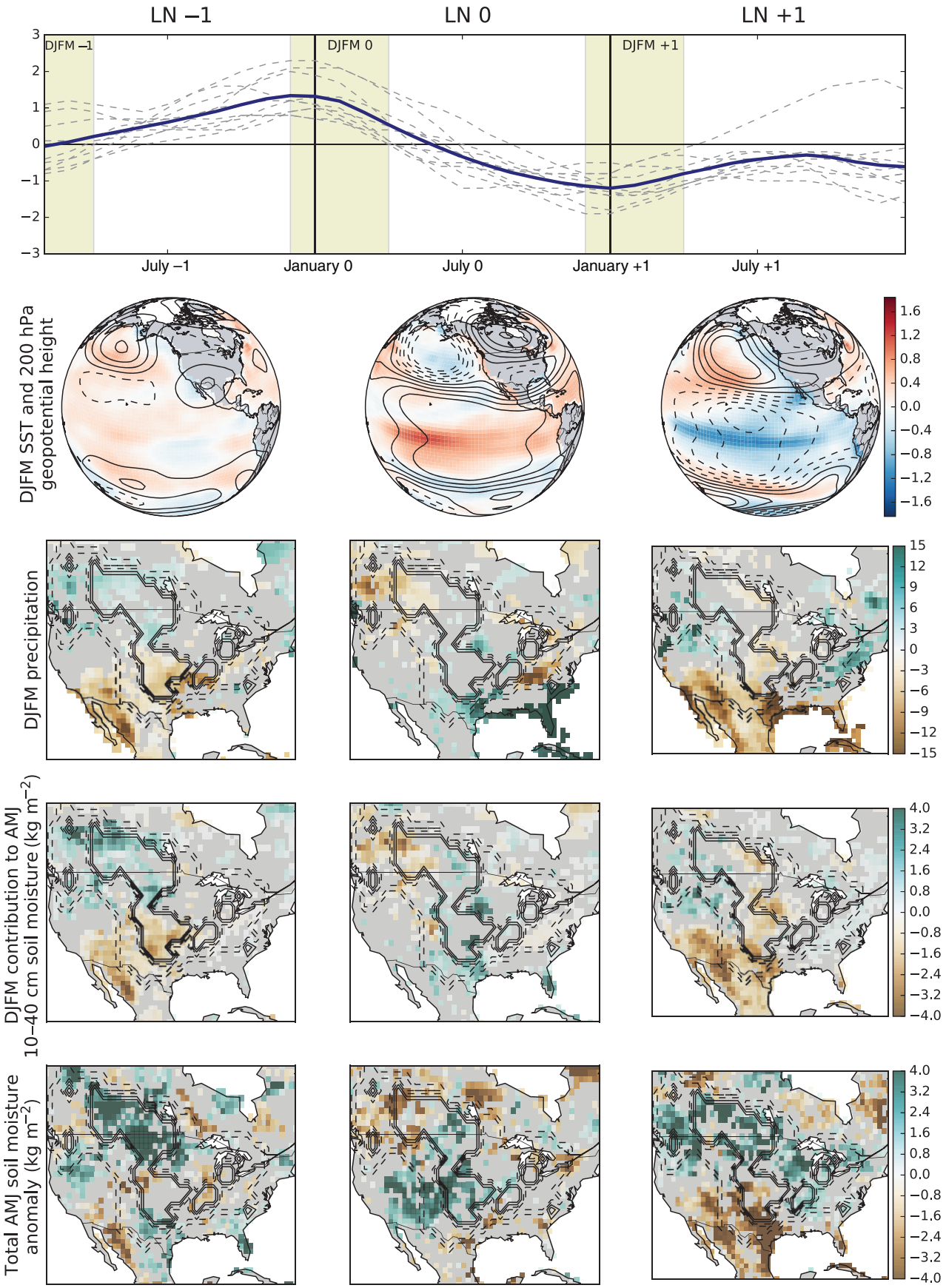

Figure 9. La Niña composite (top row), shading indicates DJFM. Sea surface temperature anomalies with contours of 200 hPa geopotential height (second row), boreal winter precipitation anomalies (third row; units of mm month^{-1}), and boreal winter precipitation contribution to springtime soil moisture (fourth row; units of kg m^{-2}) with contours indicating major (solid) and minor (dashed) wheat growing areas. Each variable is depicted for DJFM −1 (left column), DJFM 0 (centre column) and DJFM +1 (right column).

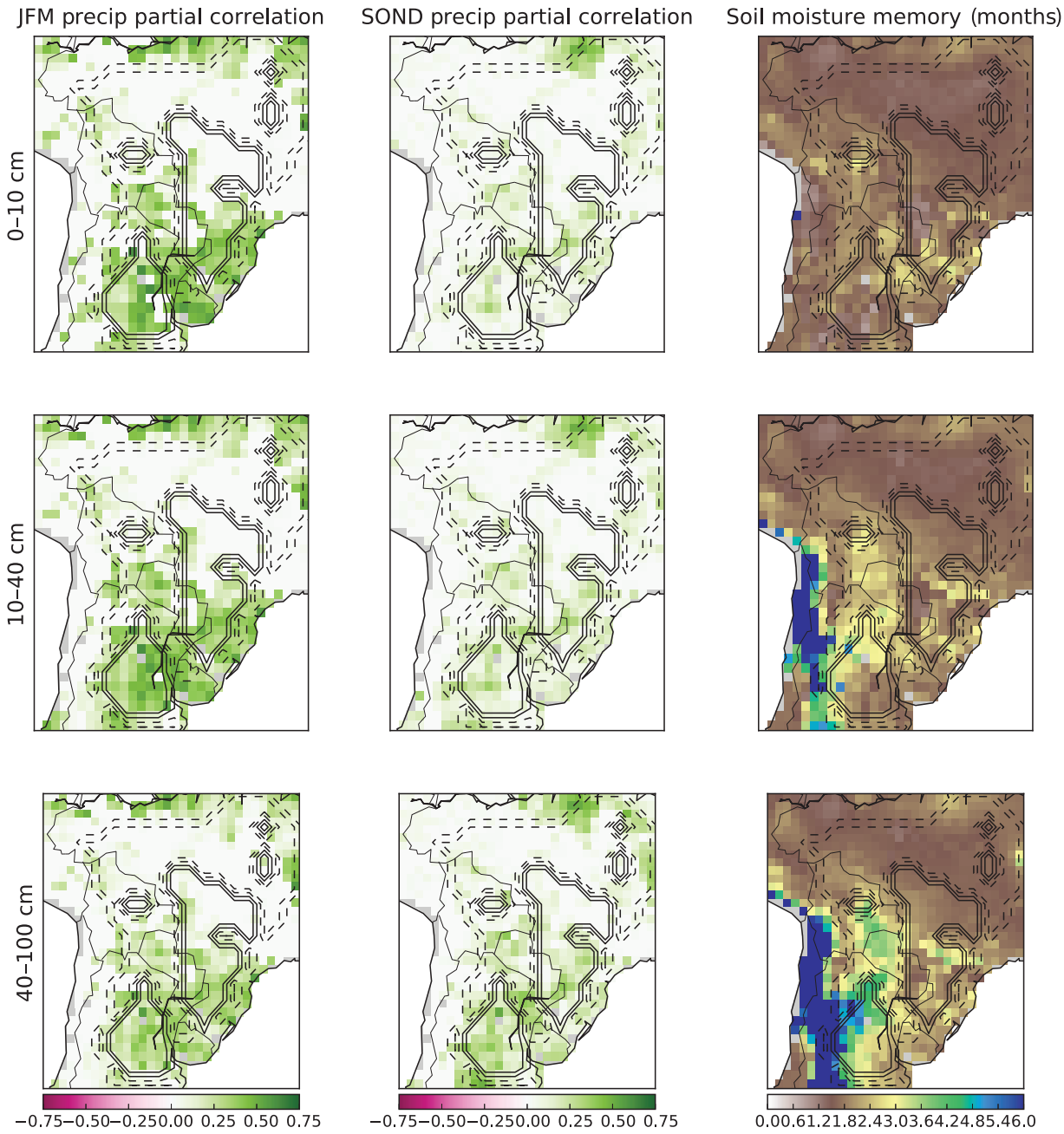

Figure 10. Statistically significant ($p < 0.1$) point-wise partial correlation between JFM soil moisture and JFM precipitation (left column) and SOND precipitation (centre column). The e-folding time in months for soil moisture anomalies in the absence of forcing (right column). Rows indicate soil moisture layer depths of 0–10 cm (top row), 10–40 cm (centre row) and 40–100 cm (bottom row). Contours indicate wheat producing areas.

in the Americas due to the dry North American wheat flowering months, which benefit from additional moisture, and the wet South American wheat flowering months, in which excess moisture leads to disease (Ferreyra *et al.*, 2001).

3.3.1. North America Yields

In the United States, both maize and soybean yields correlate with flowering season SST anomalies while wheat correlates with SSTs from the previous boreal winter (see Table 3). This is consistent with our teleconnection analysis and with previous studies on soybean (Iizumi *et al.*, 2014) and maize (Handler, 1984; Izaurralde *et al.*, 1999; Legler and Bryant, 1999; Phillips *et al.*, 1999; Wannebo and Rosenzweig, 2003), summarized in Table 1. In contradiction, Iizumi *et al.* (2014) find that both El Niño and La Niña events decrease maize yield in the US, although their analysis is based on only 20 years of data. Similarly, the discrepancy between our results and those of Legler and Bryant (1999) for soybean is likely a result of analysis structure. Legler and Bryant (1999) analyse spatial patterns of yield anomalies for crops during the growing season following an ENSO event. Our results indicate that for soybean and maize, yield anomalies are most strongly correlated with flowering season SST anomalies during developing ENSO events (EN 0) rather

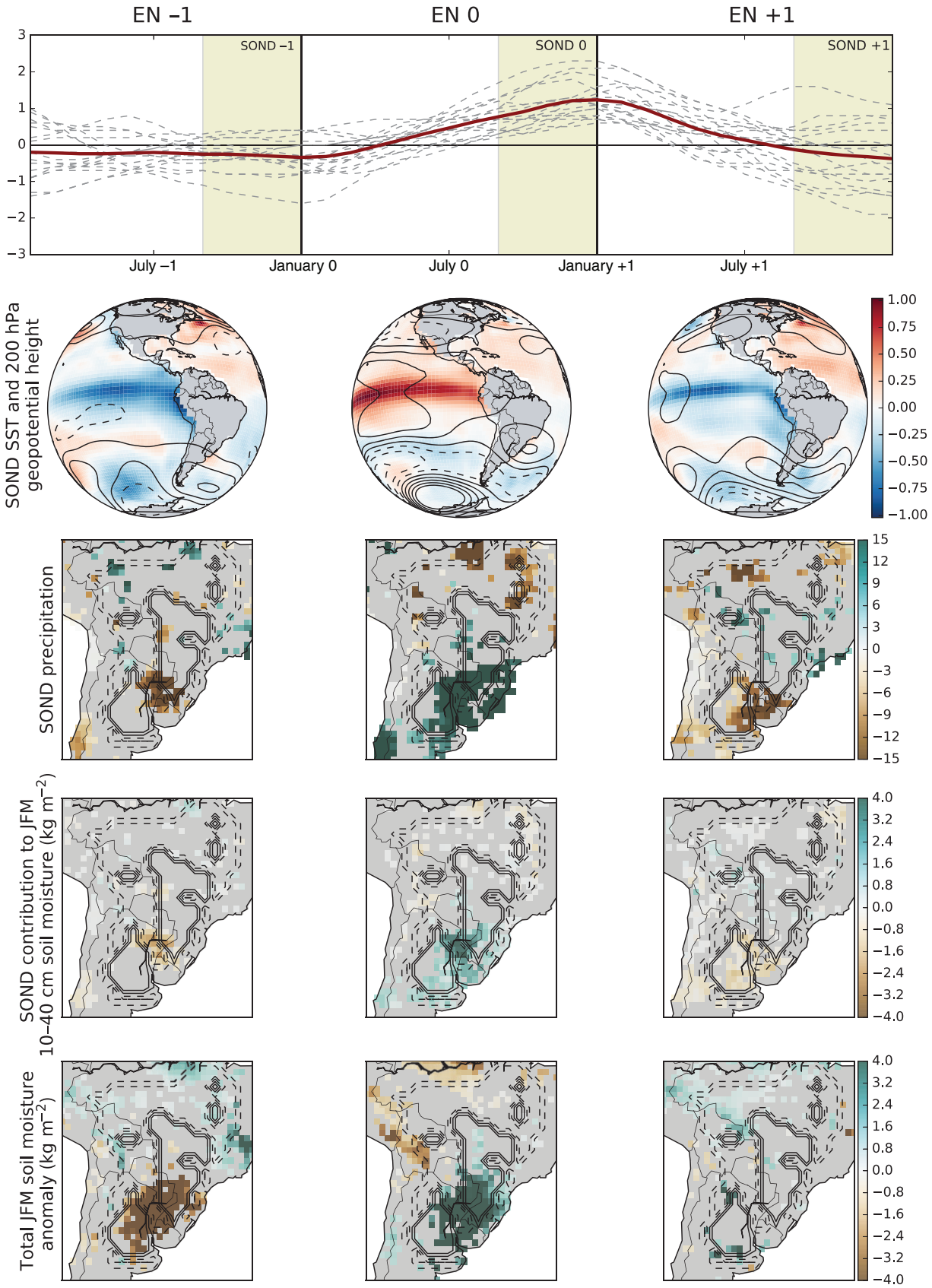

Figure 11. El Niño composite (top row), shading indicates SOND. Sea surface temperature anomalies with contours of 200 hPa geopotential height (second row), boreal winter precipitation anomalies (third row; units of mm month^{-1}), and boreal winter precipitation contribution to springtime soil moisture (fourth row; units of kg m^{-2}) with contours indicating major (solid) and minor (dashed) soybean growing areas. Each variable is depicted for SOND −1 (left column), SOND 0 (centre column) and SOND +1 (right column).

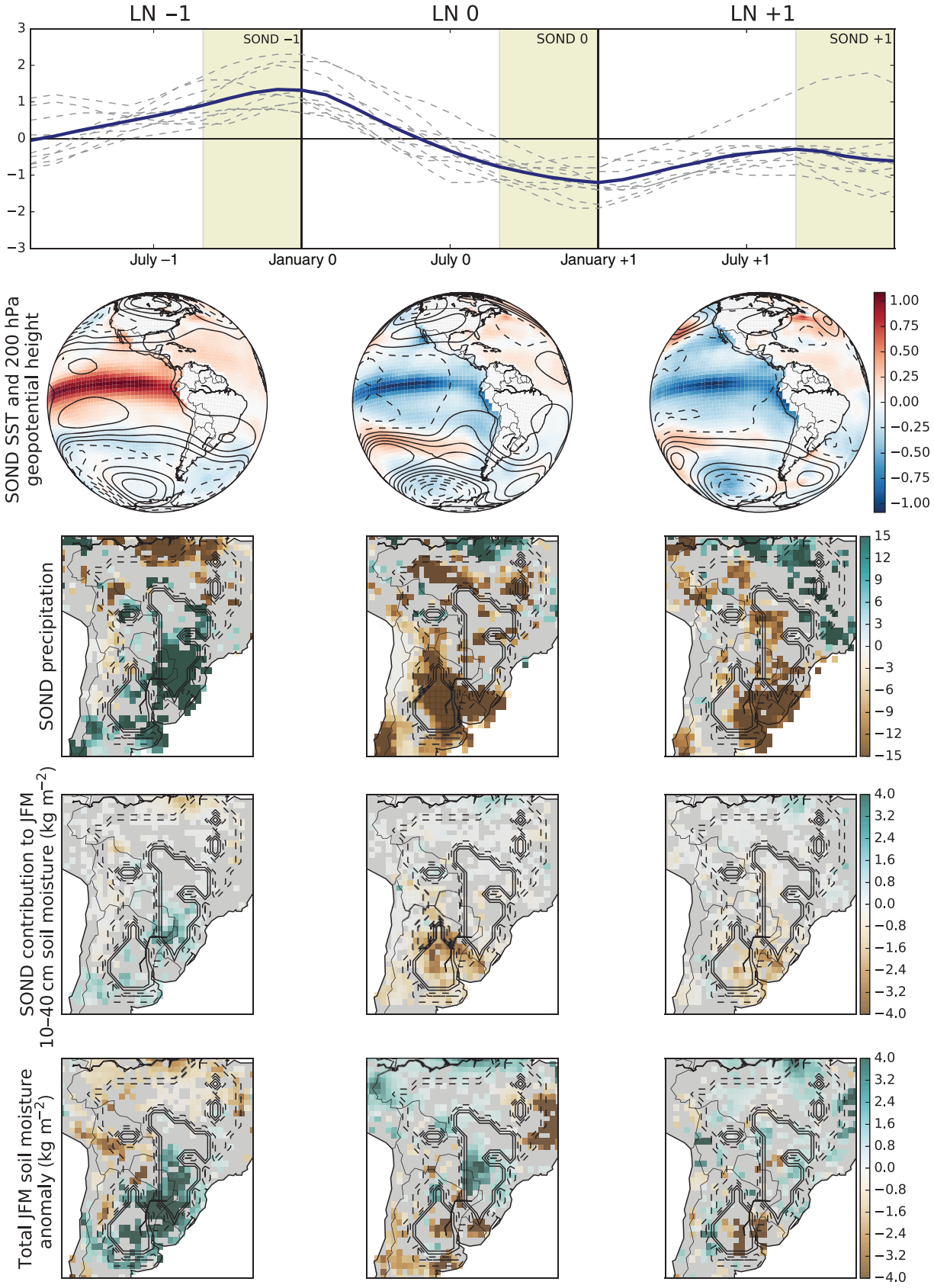

Figure 12. La Niña composite (top row), shading indicates SOND. Sea surface temperature anomalies with contours of 200 hPa geopotential height (second row), boreal winter precipitation anomalies (third row; units of mm month^{-1}), and boreal winter precipitation contribution to springtime soil moisture (fourth row; units of kg m^{-2}) with contours indicating major (solid) and minor (dashed) soybean growing areas. Each variable is depicted for SOND −1 (left column), SOND 0 (centre column) and SOND +1 (right column).

Table 3. Statistically significant ($p < 0.1$) correlations between the Oceanic Niño Index (with the month chosen based on the teleconnection analysis) and yield anomalies in major producing states/provinces.

Crop	Country	State/province	Percent of national production (%)	Correlation coefficient	ONI month
Wheat	AR	Cordoba	11.3	−0.42	October
		Santa Fe	11.5	−0.30	
		Santiago del Estero	5.1	−0.34	
	US	Kansas	16.6	0.26	December
		Nebraska	3.0	0.26	
		Oklahoma	5.5	0.31	
		Texas	5.7	0.42	
Maize	AR	Buenos Aires	35.8	0.31	December
		Cordoba	24.9	0.27	
		Santa Fe	15.4	0.41	
	BR	Sao Palo	7.5	0.39	December
		Parana	21.3	0.34	
	US	Illinois	15.7	0.21	July
		Indiana	7.2	0.22	
		Iowa	17.3	0.24	
		Michigan	2.5	0.24	
		South Dakota	4.6	0.23	
Soybean	AR	Buenos Aires	31.7	0.32	November
	US	Illinois	14.0	0.24	July
		Indiana	7.8	0.30	
		Iowa	14.9	0.22	
		Kansas	4.2	0.23	
		Missouri	6.3	0.26	
		Nebraska	8.0	0.25	
		South Dakota	4.7	0.19	

than decaying events (EN +1). This discrepancy draws attention to the importance of considering ENSO from a life-cycle perspective. There are few studies that analyse connections between ENSO and wheat in the United States, but our results agree with those of Mauget and Upchurch (1999), who also come to the conclusion that US wheat yields are correlated with previous season SST anomalies.

Results for Mexico were not statistically significant in major producing regions and mixed in sign for minor production regions, as has been found in previous analyses Dilley, 1997; López *et al.*, 2003). We similarly found no statistically significant correlations between wheat yields in Canada and tropical SST anomalies, which is somewhat in contrast to Hsieh *et al.* (1999) who found a tenuous linear correlation in the tropics and that both the nine highest and lowest yield years were associated with negative SST anomalies. This discrepancy points to the complexity of the climate-crop relation in Canada, and a need for further study.

3.3.2. South America Yields

Significant correlations exist only in Argentina for wheat and soybean yield anomalies, but correlations with maize yield anomalies exist in both Argentina and Brazil. Consistent with both the location of precipitation teleconnections and with past literature (Iizumi *et al.*, 2014), a negative correlation exists between wheat yield anomalies and El Niño in Argentina. However, maize yield anomalies in Argentina and Brazil are positively correlated with El Niño, which reflects that while precipitation is necessary during the drier NDJ months, excess precipitation in wet SON months during El Niños leads to increased plant disease for wheat. These results agree with those of Ferreyra *et al.* (2001); Podestá *et al.* (1999) and Iizumi *et al.* (2014) (see Table 1). The positive correlation between soybean yield anomalies in Argentina and the El Niño index from the preceding boreal winter is consistent with, and reflects the combined influence of precipitation teleconnections and soil moisture memory as we demonstrated in the lagged teleconnection analysis. While we found no significant correlations in the south of Brazil, previous studies of the region have found relationships between crop yields and ENSO (Belrato and Fontana, 2001; Cunha, 2001; Cunha *et al.*, 2001; Berlato *et al.*, 2005), although they did not report levels of significance. The results of those studies are consistent with the climate teleconnections outlined in this paper, and are of the same sign as the yield anomalies found for Argentina: during El Niño conditions are unfavourable for wheat in the south of Brazil but favourable for both maize and soybean. The reverse holds true during La Niña.

3.3.3. Life cycles of yield anomalies

To evaluate the magnitude and timing of the impact of ENSO on crop yields, we binned yield anomalies by ENSO phase. We grouped the yield of states that are correlated with ENSO into years corresponding to phases of the El Niño and La Niña life cycles. Doing so demonstrates that ENSO exhibits a sufficiently strong influence on growing conditions in these regions to force a progression in yield anomalies that reflect the ENSO life

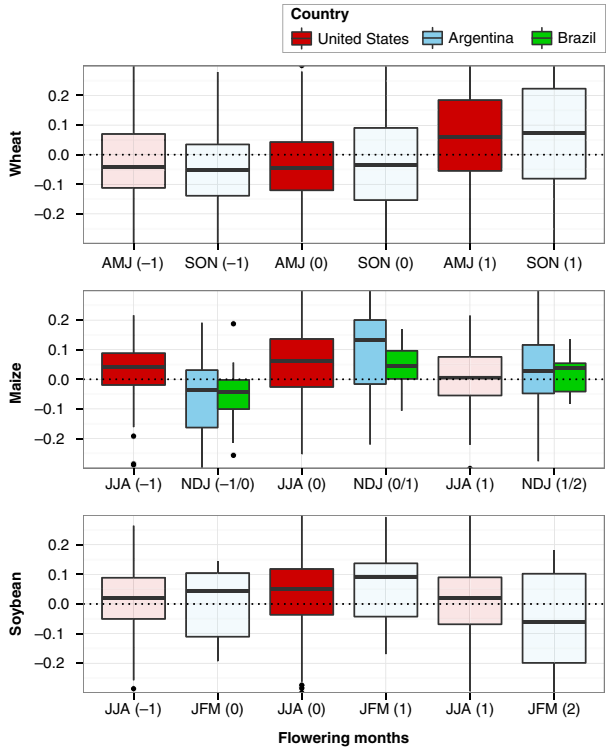

Figure 13. Life cycle of yield anomalies (calculated as a fraction of expected yield) for states from Table 3 during an El Niño life cycle. Solid shading indicates that the anomalies are significantly different from zero ($p < 0.1$), transparent shading indicates that the yield anomalies are not significantly different from zero.

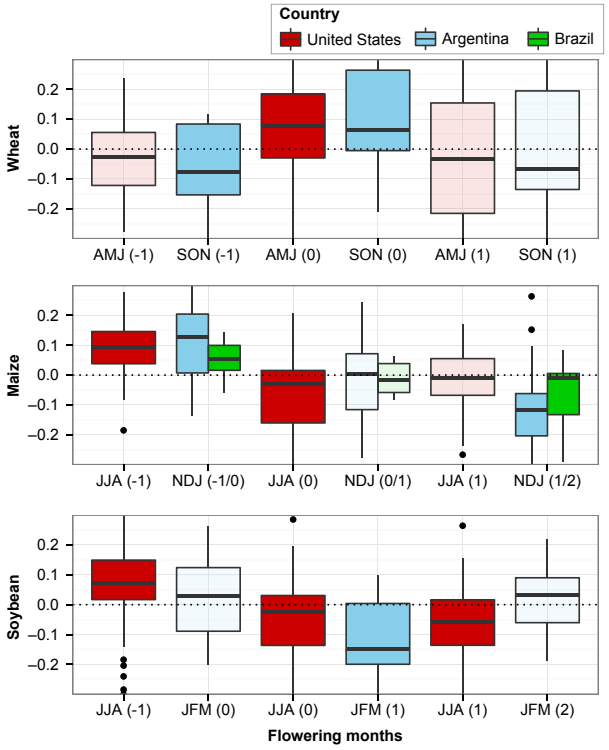

Figure 14. Life cycle of yield anomalies (calculated as a fraction of expected yield) for states from Table 3 during a La Niña life cycle. Solid shading indicates that the anomalies are significantly different from zero ($p < 0.1$), transparent shading indicates that the yield anomalies are not significantly different from zero.

cycle. The progression of yield anomalies is generally more clear during the La Niña life cycle than the El Niño life cycle (see Figures 13 and 14). Teleconnections in both ENSO life cycles tend to force same-sign yield anomalies across North and South America within a cropping year.

The same-sign yield variability is attributable primarily to same-season teleconnections for maize – and therefore may be obvious from the perspective of agricultural management – but is the combined result of same-season and lagged teleconnections for wheat and soybean. As an illustration of how the phasing of teleconnections and flowering seasons leads to same-sign yield variability, we will first consider a series of yield anomalies for wheat. Following the peak of an El Niño, positive precipitation anomalies in the southern Great Plains from the previous boreal winter force positive flowering season soil moisture anomalies (EN 1 in Figure 8 and LN 0 in Figure 9), which increases wheat yields (AMJ 1 in Figure 13, AMJ 0 in Figure 14). Drier than normal conditions then develop in South America due to negative SST anomalies (LN 0, Figure 3) and force positive yield anomalies due to reduced disease (SON 1 in Figure 13., SON 0 in Figure 14). If we follow the same analysis for soybean yield anomalies during the La Niña life cycle, same-season teleconnections force negative yield anomalies during JJA 0 and JJA 1 in the United States (see teleconnections in Figure 6, yield anomalies in Figure 14) and lagged teleconnections force negative yield anomalies in JFM 1 due to precipitation deficits from SOND 0 (see Argentina teleconnections in Figure 12 and yield anomalies in Figure 14). The comparable progression for maize is more straightforward because it is purely same-season teleconnections that are important for yield anomalies, which are strongest during the warm phase of ENSO (JJA 0 and NDJ 0/1 in Figure 13; JJA −1 and NDJ −1/0 in Figure 14).

3.3.4. *Conclusions*

ENSO significantly affects crop yields in North and South America through both same-season and lagged teleconnections. Same-season temperature and precipitation teleconnections explain ENSO's influence on maize and soybean yields in North America as well as wheat and maize yields in South America. Soil moisture anomalies forced by previous season precipitation teleconnections are important for wheat yields in the United States and soybean yields in Argentina.

In the United States, maize and soybean yields are positively correlated with flowering season SST anomalies while wheat yields are positively correlated with previous boreal winter SSTs. These results are consistent with yields responding positively to increased precipitation. In the summer of a developing La Niña, teleconnections elevate maximum temperatures and decrease precipitation over major crop-producing regions of the United States such that they negatively affect maize and soybean yields.

Wheat yields are primarily affected by boreal wintertime teleconnections from the previous season when ENSO exhibits a much stronger influence on precipitation. Soil moisture memory in the United States acts to translate ENSO-induced winter precipitation anomalies into spring growing season soil moisture anomalies, particularly in the southern Great Plains. Hence US wheat yields tend to increase following El Niño conditions in the preceding winter.

ENSO crop correlations over southeast South America in SON and NDJ are a direct result of ENSO precipitation teleconnections overlaid on seasonal climatology. ENSO induces a circulation anomaly centred over southeast South America that forces precipitation anomalies during wheat (SON) and maize (NDJ) flowering seasons. In the relatively wet months of wheat flowering, increased precipitation leads to a higher probability of disease and decreased yields. In the drier months of maize and soybean flowering, additional precipitation likely increases yields. Correlations between El Niño and yield, therefore, are consistently negative for wheat but positive for maize. During the soybean flowering season in Argentina, lagged teleconnections become important. Soil moisture memory in parts of Argentina sustains moisture anomalies from SOND into JFM, which affects soybean yields.

An ENSO life cycle is evident not only in SST anomalies and teleconnections, but also in a sequence of positive and negative crop yield anomalies. The pattern is more obvious in the yield anomalies forced by the La Niña life cycle than those forced by the El Niño life cycle. Teleconnections from both ENSO life cycles, however, tend to impose same-sign yield anomalies across North and South America, which implies that El Niño and La Niña life cycles can drive progressive sequences of Pan-American yield anomalies. While the magnitude of the yield anomalies forced by ENSO are often modest, the fact that these anomalies occur in major production regions means that they can have a significant effect on global markets. This information may be leveraged to improve food security not only in crop-producing countries, but also in import-dependent countries and more generally used as a tool to understand variability in crop production.

Acknowledgements

This material is based upon the work supported by the National Science Foundation Graduate Research Fellowship under grant no. DGE-16-44869. RS acknowledges the support from NSF award AGS-1401400. NCEP Reanalysis and GPCC data were provided by the NOAA/OAR/ESRL PSD from their website at http://www.esrl.noaa.gov/psd/. Soil moisture data used in this study was archived and distributed by the Goddard Earth Sciences Data and Information Services Center. The authors would like to thank two anonymous reviewers for their helpful comments.

References

Alexander MA, Bladé I, Newman M, Lanzante JR, Lau N-C, Scott JD. 2002. The atmospheric bridge: the influence of ENSO teleconnections on air–sea interaction over the global oceans. *J. Clim.* **15**(16): 2205–2231, doi: 10.1175/1520-0442(2002)015<2205:TABTIO>2.0.CO;2.

Anderson W, You L, Wood S, Wood-Sichra U, Wu W. 2015. An analysis of methodological and spatial differences in global cropping systems models and maps. *Glob. Ecol. Biogeogr.* **24**(2): 180–191.

Barnabás B, Jäger K, Fehér A. 2008. The effect of drought and heat stress on reproductive processes in cereals. *Plant Cell Environ.* **31**: 11–38, doi: 10.1111/j.1365-3040.2007.01727.x.

Belrato M, Fontana DC. 2001. Impacts of el niño and la niña on agricultural production in southern brazil and the use of climate forecasts in agriculture. In *Applications of Climate Forecasting for Better Decision-Making Processes in Agriculture*, Cunha GR, Haas JC, Berlato MA (eds). Embrapa Trigo: Passo Fundo, Brazil, 217–241.

Berlato MA, Farenzena H, Fontana DC. 2005. Association between El Nino Southern Oscillation and corn yield in Rio Grande do Sul state. *Pesq. Agropec. Bras.* **40**(5): 423–432.

Bjerknes J. 1969. Atmospheric teleconnections from the equatorial Pacific. *Mon. Weather Rev.* **97**(3): 163–172, doi: 10.1175/1520-0493(1969)097<0163:ATFTEP>2.3.CO;2.

Capotondi A, Wittenberg AT, Newman M, Di Lorenzo E, Yu JY, Braconnot P, Cole J, Dewitte B, Giese B, Guilyardi E, Jin FF. 2015. Understanding ENSO diversity. *Bull. Am. Meteorol. Soc.* **96**(6): 921–938.

Cazes-Boezio G, Robertson AW, Mechoso CR. 2003. Seasonal dependence of ENSO teleconnections over South America and relationships with precipitation in Uruguay. *J. Clim.* **16**: 1159–1176, doi: 10.1175/1520-0442(2003)16<1159:SDOETO>2.0.CO;2.

Cunha GR. 2001. El Niño Southern Oscillation and climate forecasts applied to crops management southern Brazil. In *Applications of Climate Forecasting for Better Decision-Making Processes in Agriculture*, Cunha GR, Haas JC, Berlato MA (eds). Embrapa Trigo: Passo Fundo, Brazil, 181–201.

Cunha G, Dalmago G, Estefanel V. 2001. El Nino – southern oscillation influences on wheat crop in Brazil. In *Wheat in a Global Environment*. Springer, 445–450.

Delworth T, Manabe S. 1993. Climate variability and land-surface processes. *Adv. Water Resour.* **16**: 3–20, doi: 10.1016/0309-1708(93)90026-C.

Diaz HF, Hoerling MP, Eischeid JK. 2001. ENSO variability, teleconnections and climate change. *Int. J. Climatol.* **21**(15): 1845–1862.

Dilley M. 1997. Climatic factors affecting annual maize yields in the valley of Oaxaca, Mexico. *Int. J. Climatol.* **17**(14): 1549–1557.

Ebisuzaki W. 1997. A method to estimate the statistical significance of a correlation when the data are serially correlated. *J. Clim.* **10**(9): 2147–2153.

FAO. 2009. High food prices: the food security crisis of 2007/2008 and recent food price increases – facts and lessons.

FAO. 2010. Food outlook, global market analysis. Global information and early warning system on food and agriculture.

Ferreyra RA, Podestá GP, Messina CD, Letson D, Dardanelli J, Guevara E, Meira S. 2001. A linked-modeling framework to estimate maize production risk associated with ENSO-related climate variability in Argentina. *Agric. For. Meteorol.* **107**(3): 177–192.

Fischer, G, Nachtergaele F, Prieler S, Van Velthuizen H, Verelst L, Wiberg D. 2008. Global agro-ecological zones assessment for agriculture (GAEZ 2008). IIASA, Laxenburg, Austria and FAO, Rome, Italy.

Fritz S, See L, McCallum I, Schill C, Obersteiner M, Van der Velde M, Boettcher H, Havlík P, Achard F. 2011. Highlighting continued uncertainty in global land cover maps for the user community. *Environ. Res. Lett.* **6**(4): 044005, doi: 10.1088/1748-9326/6/4/044005.

Grimm AM, Barros VR, Doyle ME. 2000. Climate variability in southern South America associated with El Niño and La Niña events. *J. Clim.* **13**(1): 35–58.

Hammer G, Holzworth D, Stone R. 1996. The value of skill in seasonal climate forecasting to wheat crop management in a region with high climatic variability. *Aust. J. Agric. Res.* **47**(5): 717–737.

Hammer G, Hansen J, Phillips J, Mjelde J, Hill H, Love A, Potgieter A. 2001. Advances in application of climate prediction in agriculture. *Agr. Syst.* **70**(2): 515–553.

Handler P. 1984. Corn yields in the United States and sea surface temperature anomalies in the equatorial Pacific Ocean during the period 1868–1982. *Agric. For. Meteorol.* **31**(1): 25–32.

Hsieh WW, Tang B, Garnett ER. 1999. Teleconnections between pacific sea surface temperatures and Canadian prairie wheat yield. *Agric. For. Meteorol.* **96**(4): 209–217.

Iizumi T, Sakuma H, Yokozawa M, Luo J-J, Challinor AJ, Brown ME, Sakurai G, Yamagata T. 2013. Prediction of seasonal climate-induced variations in global food production. *Nat. Clim. Change* **3**(10): 904–908, doi: 10.1038/nclimate1945.

Iizumi T, Luo J-J, Challinor AJ, Sakurai G, Yokozawa M, Sakuma H, Brown ME, Yamagata T. 2014. Impacts of El Niño Southern Oscillation on the global yields of major crops. *Nat. Commun.* **5**: 3712, doi: 10.1038/ncomms4712.

Izaurralde R, Rosenberg N, Brown R, Legler D, López MT, Srinivasan R. 1999. Modeled effects of moderate and strong Los Niños' on crop productivity in North America. *Agric. For. Meteorol.* **94**(3): 259–268.

Kalnay E, Kanamitsu M, Kistler R, Collins W, Deaven D, Gandin L, Iredell M, Saha S, White G, Woollen J, Zhu Y. 1996. The NCEP/NCAR 40-year reanalysis project. *Bull. Am. Meteorol. Soc.* **77**(3): 437–471.

Kumar A, Hoerling MP. 1998. Annual cycle of Pacific-North American seasonal predictability associated with different phases of ENSO. *J. Clim.* **11**(12): 3295–3308.

Legler DM, Bryant KJ. 1999. Impact of ENSO-related climate anomalies on crop yields in the U.S. *Clim. Change* **42**: 351–375.

Lobell DB, Hammer GL, McLean G, Messina C, Roberts MJ, Schlenker W. 2013. The critical role of extreme heat for maize production in the United States. *Nat. Clim. Change* **3**(5): 497–501.

Lobell DB, Roberts MJ, Schlenker W, Braun N, Little BB, Rejesus RM, Hammer GL. 2014. Greater sensitivity to drought accompanies maize yield increase in the US Midwest. *Science* **344**(6183): 516–519.

López MT, Izaurralde C, Rosenberg NJ, González ADB, Garca JS. 2003. Modeling El Niño southern oscillation climate impact on Mexican agriculture. *Geofis. Int.* **42**(3): 331–340.

Mason SJ, Goddard L. 2001. Probabilistic precipitation anomalies associated with ENSO. *Bull. Am. Meteorol. Soc.* **82**(4): 619–638.

Mauget SA, Upchurch DR. 1999. El Niño and La Niña related climate and agricultural impacts over the Great Plains and Midwest. *J. Prod. Agric.* **12**(2): 203–215.

Messina CD, Hansen JW, Hall AJ. 1999. Land allocation conditioned on El Niño-Southern Oscillation phases in the Pampas of Argentina. *Agr. Syst.* **60**: 197–212.

Mo KC, Paegle JN. 2001. The Pacific-South American modes and their downstream effects. *Int. J. Climatol.* **21**(10): 1211–1229.

Okumura YM, Deser C. 2010. Asymmetry in the duration of El Niño and La Niña. *J. Clim.* **23**(21): 5826–5843, doi: 10.1175/2010JCLI3592.1.

Phillips J, Rajagopalan B, Cane M, Rosenzweig C. 1999. The role of ENSO in determining climate and maize yield variability in the U.S. cornbelt. *Int. J. Climatol.* **19**: 877–888, doi: 10.1002/(SICI)1097-0088(19990630)19:8<877::AID-JOC406>3.0.CO;2-Q.

Podestá GP, Messina CD, Grondona MO, Magrin GO. 1999. Associations between grain crop yields in Central-Eastern Argentina and El Niño-Southern Oscillation. *J. Appl. Meteorol.* **38**(10): 1488–1498, doi: 10.1175/1520-0450(1999)038<1488:ABGCYI>2.0.CO;2.

Podesta G, Letson D, Messina C, Royce F, Ferreyra RA, Jones J, Hansen J, Llovet I, Grondona M, O'Brien JJ. 2002. Use of ENSO-related climate information in agricultural decision making in Argentina: a pilot experience. *Agr. Syst.* **74**(3): 371–392.

Portmann FT, Siebert S, Döll P. 2010. MIRCA2000 – global monthly irrigated and rainfed crop areas around the year 2000: a new high-resolution data set for agricultural and hydrological modeling. *Global Biogeochem. Cycles* **24**(1): GB1011, doi: 10.1029/2008GB003435.

Rasmusson E, Carpenter T. 1982. Variations in tropical sea surface temperature and surface wind fields associated with the Southern Oscillation/El Nino. *Mon. Weather Rev.* **110**: 354–384.

Rodell M, Kato Beaudoing H. 2015. GLDAS Noah Land Surface Model L4 monthly 1.0×1.0 degree Version 2.0. Technical Report, NASA/GSFC/HSL (12.01.2013), Greenbelt, Maryland, USA: Goddard Earth Sciences Data and Information Services Center (GES DISC). doi: 10.5067/QN80TO7ZHFJZ.

Schlenker W, Roberts MJ. 2006. Nonlinear effects of weather on corn yields. *Appl. Econ. Perspect. Policy* **28**(3): 391–398.

Schlenker W, Roberts MJ. 2009. Nonlinear temperature effects indicate severe damages to us crop yields under climate change. *Proc. Natl. Acad. Sci. USA* **106**(37): 15594–15598.

Schneider U, Becker A, Finger P, Meyer-Christoffer A, Rudolf B, Ziese M. 2011. GPCC Full Data Reanalysis Version 6.0 at 1.0 Degree: Monthly Land-Surface Precipitation from Rain-Gauges Built on GTS-based and Historic Data.

Schubert SD, Suarez MJ, Pegion PJ, Koster RD, Bacmeister JT. 2004. Causes of long-term drought in the US Great Plains. *J. Clim.* **17**(3): 485–503.

Smith TM, Reynolds RW, Peterson TC, Lawrimore J. 2008. Improvements to NOAA's historical merged land-ocean surface temperature analysis (1880-2006). *J. Clim.* **21**(10): 2283–2296.

Thompson C, Battisti D. 2000. A linear stochastic dynamical model of ENSO. Part I: model development. *J. Clim.* **13**(15): 2818–2832.

Trenberth KE, Branstator GW, Karoly D, Kumar A, Lau N-C, Ropelewski C. 1998. Progress during TOGA in understanding and modeling global teleconnections associated with tropical sea surface temperatures. *J. Geophys. Res. Oceans* **103**(C7): 14291–14324.

Vinnikov KY, Robock A, Speranskaya NA, Schlosser CA. 1996. Scales of temporal and spatial variability of midlatitude soil moisture. *J. Geophys. Res.* **101**: 7163, doi: 10.1029/95JD02753.

Wang C, Picaut J. 2004. Understanding ENSO physics – a review. *Geophys. Monogr. Ser.* **147**: 21–48, doi: 10.1029/GM147.

Wannebo A, Rosenzweig C. 2003. Remote sensing of US cornbelt areas sensitive to the El Niño-Southern Oscillationo-Southern Oscillation. *Int. J. Remote Sens.* **24**(10): 2055–2067.

Wilks DS. 2011. *Statistical Methods in the Atmospheric Sciences*, Vol. **100**. Academic Press.

You L, Wood S, Wood-Sichra U, Wu W. 2014. Generating global crop distribution maps: grom census to grid. *Agr. Syst.* **127**: 53–60, doi: 10.1016/j.agsy.2014.01.002.

